Atmos. Chem. Phys. Discuss., 15, 3577–3627, 2015
www.atmos-chem-phys-discuss.net/15/3577/2015/
doi:10.5194/acpd-15-3577-2015

Atmospheric Chemistry and Physics Discussions
Open Access

Predicting the mineral composition of dust aerosols – Part 2: Model evaluation and identification of key processes with observations

J. P. Perlwitz[1,2], C. Pérez García-Pando[1,2], and R. L. Miller[2,1]

[1]Department of Applied Physics and Applied Mathematics, Columbia University in The City of New York, New York, USA
[2]NASA Goddard Institute for Space Studies, New York, New York, USA

Received: 17 December 2014 – Accepted: 12 January 2015 – Published: 6 February 2015

Correspondence to: J. P. Perlwitz (jan.p.perlwitz@nasa.gov)

Published by Copernicus Publications on behalf of the European Geosciences Union.

Abstract

A global compilation from nearly sixty measurement studies is used to evaluate two methods of simulating the mineral composition of dust aerosols in an Earth system model. Both methods are based upon a Mean Mineralogical Table (MMT) that relates the soil mineral fractions to a global atlas of arid soil type. The Soil Mineral Fraction (SMF) method assumes that the aerosol mineral fractions match those of the soil. The MMT is based upon soil measurements after wet sieving, where soil aggregates are broken into smaller particles. The second method approximately reconstructs the aggregates and size distribution of the original soil that is subject to wind erosion. This model is referred to as the Aerosol Mineral Fraction (AMF) method because the mineral fractions of the aerosols differ from those of the wet-sieved parent soil, partly due to reaggregation. The AMF method remedies some of the deficiencies of the SMF method in comparison to observation. Only the AMF method restores phyllosilicate mass to silt sizes, where they are abundant according to observations. In addition, the AMF quartz fraction of silt particles is in closer agreement with measured values, in contrast to the overestimated SMF fraction. Measurements at separate clay and silt particle sizes are shown to be more useful for evaluation of the models, compared to the sum over all particles sizes that is susceptible to compensating errors in the SMF experiment. Model errors suggest that apportionment of the emitted silt fraction of each mineral into the corresponding transported size categories is an important remaining uncertainty. Substantial uncertainty remains in evaluating both models and the MMT due to the limited number of size-resolved measurements of mineral content that sparsely sample aerosols from the major dust sources. The importance of climate processes dependent upon aerosol mineral composition shows the need for global and routine mineral measurements.

ACPD
15, 3577–3627, 2015

1 Introduction

The effect of dust aerosols upon climate is strongly dependent upon the particle mineral composition (see Perlwitz et al., 2015, and references therein). Despite this, the radiative and chemical properties of dust aerosols are nearly always assumed by Earth system models to be globally uniform and independent of their source region.

Claquin et al. (1999) provided the first global estimate of soil mineral content by relating it to soil type, whose regional distribution is given by the Digital Soil Map of the World (DSMW; FAO, 2007; FAO/IIASA/ISRIC/ISSCAS/JRC, 2012). Nickovic et al. (2012) and Journet et al. (2014) extended this approach by including additional soil types, measurements and minerals. Deriving the mineral composition of emitted aerosols presents additional challenges. Claquin et al. (1999) note that measurements of soil type that are the basis of global datasets are based on wet sedimentation (or "wet sieving") techniques that disturb the soil samples, breaking the aggregates that are found in the original, undispersed soil that is subject to wind erosion. Wet-sieving alters the soil size distribution, replacing aggregates with a collection of smaller and relatively loose particles (Shao, 2001; Choate et al., 2006; Laurent et al., 2008). In the absence of measurements of the undisturbed soil, studies have assumed that the size distribution of the emitted minerals resemble those of the wet-sieved parent soil (Hoose et al., 2008; Atkinson et al., 2013; Journet et al., 2014). An additional challenge is how to treat particles that are combinations of different minerals. For example, iron oxides are often observed as small impurities attached to particles comprised predominately of other minerals (e.g. Scheuvens and Kandler, 2014). These mixed particles have roughly half the density of pure iron oxides, and thus carry iron farther downwind of its source. Finally, refinement of models is challenged by limited global measurements of size-resolved aerosol composition. Much of the available measurements are from field campaigns or ship cruises of limited duration, while changes in the sampling and analysis methods through time have resulted in additional uncertainty.

ACPD
15, 3577–3627, 2015

We address the first two challenges in a companion paper (Perlwitz et al., 2015), where we describe a new approach to estimate aerosol mineral content by extending the method that provides the composition of a wet-sieved soil (Claquin et al., 1999). We reconstruct the undispersed size distribution of the original soil that is subject to wind erosion, and apply an empirical constraint upon the relative emission of clay and silt that further differentiates the soil and aerosol mineral content. We also propose a method for mixing minerals with small impurities of iron oxides. In the companion article, we compare regional variations of mineral emission and concentration calculated by our model and a baseline model that assumes the aerosol mineral fractions are identical to those of the wet-sieved parent soil. We perform a limited comparison to size-resolved measurements from North Africa, showing that our extensions bring the model into better agreement.

In this article, we compare our models' aerosol mineral content to a new global compilation of observations from almost sixty citations. In Sect. 2, we summarize our new modeling approach and the simulations performed with the NASA Goddard Institute for Space Studies (GISS) Earth System ModelE, whose details can be found in Perlwitz et al. (2015). Section 3 presents our compilation of measurements for model evaluation (that is available in Table S1 of the Supplement), while Sect. 4 describes the evaluation approach. In Sect. 5 we discuss the results of the evaluation in terms of mineral fractions, ratios and size distribution. Our conclusions and recommendations are presented in Sect. 6.

2 Model simulations

Simulations are performed with the NASA GISS ModelE using a resolution of 2° latitude by 2.5° longitude covering the years 2002 to 2010. This period was chosen to coincide with the detailed measurement record at Izaña that is analyzed separately (Pérez García-Pando et al., 2015), but overlaps with many of the measurements used for evaluation in the present study. The horizontal winds at each level of the model are

ACPD
15, 3577–3627, 2015

nudged every six hours toward the NCEP reanalyzed values (Kalnay et al., 1996). This increases the resemblance of model transport to that observed so that the mineral fractions simulated at the observing sites are more strongly dependent upon our treatment of aerosol emission and removal. Similarly, we prescribe atmospheric composition, sea surface temperature and sea ice based upon observed values (e.g. Rayner et al., 2003). Dust radiative forcing is calculated from a climatological background distribution whose particle optical properties are assumed to be regionally invariant. Calculation of radiative forcing by the individual minerals included in this study is deferred to a later time.

Two experiments will be compared to our compilation of observations. These experiments are more fully described in Perlwitz et al. (2015), but their main features are given here. In the baseline or control experiment, the soil mineral fractions of the wet-sieved parent soil are calculated using a global atlas of arid soil type and the Mean Mineralogical Table (MMT) constructed by Claquin et al. (1999). The MMT gives the soil fractions of phyllosilicates (illite, kaolinite, and smectite) along with quartz and calcite in the clay-size range (whose diameters are less than 2 µm). Similarly, at silt sizes (with diameters between 2 and 50 µm), the MMT gives the fractions of quartz and calcite along with feldspar, gypsum and hematite. In the remainder of this study, we refer to the latter mineral more generally as "iron oxide". Similarly, we refer to calcite as "carbonate". Following Nickovic et al. (2012), we extend iron oxides into the clay-sized range by assuming that their fraction is identical to their MMT value at silt sizes. The mineral fractions provided for each size class by the MMT are combined with the fraction of each size class provided by the FAO soil texture atlas. This gives the mineral fractions of the wet-sieved soil at each location. For our baseline experiment, we assume that the aerosol mineral fractions are identical to the soil mineral fractions that vary with the local soil type and texture. We refer to this experiment as the Soil Mineral Fraction (SMF) version.

After emission, the minerals are transported within five size classes extending between 0.1 and 32 µm. For silt particles, the MMT gives the fraction of each mineral

ACPD
15, 3577–3627, 2015

summed over the entire size range (between 2 and 50 µm). It remains to distribute this fraction over the four silt-size categories transported by the model. In the absence of size-resolved measurements of emission for individual minerals, we use the size distribution of surface concentration measured for each mineral at Tinfou, Morocco by Kandler et al. (2009). The size distribution of surface concentration is influenced by deposition, and the largest particles are removed preferentially by gravitational setting. Thus, our use of surface concentration to apportion emission within the silt size category may underestimate emission of the largest sized particles. In fact, Perlwitz et al. (2015) show that our model underestimates the aerosol fraction of all minerals at Tinfou for the largest silt size category (their Fig. 18), suggesting that our emission of this size is underestimated. Because the size-resolved fractions derived from surface concentration are normalized, underestimated emission of the largest silt particles would correspond to an overestimate of the emitted fraction of the smallest silt particles. We will return to the effect of this potential bias when we evaluate the model with observations.

Our second experiment is movitated by measurements showing significant differences between the size-resolved mineral fractions of the wet-sieved soil and the resulting aerosol concentration. We extend the baseline method by first reconstructing the original size distribution of the soil prior to wet sieving. We reconstruct silt-sized aggregates in proportion to the clay-sized minerals present in the wet-sieved soil, using an empirical coefficient of proportionality γ that controls the amount of reaggregation. The reconstructed silt fraction is thus a combination of silt-sized particles in the wet-sieved soil along with aggregates that were converted into clay-sized particles during sieving. As a consequence, phyllosilicate minerals (illite, kaolinite and smectite) that are nominally "clay" minerals are more prevalent at silt sizes, consistent with aerosol measurements (Kandler et al., 2009), even though they are absent in a soil whose aggregates are dispersed by wet sieving (Claquin et al., 1999).

In addition, we account for the transformation of the mineral fractions during the emission process. We constrain the emitted clay and silt-sized fractions with measured

ACPD
15, 3577–3627, 2015

size distributions of aerosol emission that have been shown to be relatively invariant up to 20 μm for a variety of soils and wind conditions (e.g. Gillette et al., 1974; Sow et al., 2009; Kok, 2011). The measured fraction of emission at clay sizes is also used to extend the size range of emitted feldspar and gypsum into clay-sized diameters. (These minerals are present only at silt sizes in the MMT and the SMF model.) Our extensions of the SMF method result in aerosol mineral fractions that are different from fractions of the wet-sieved parent soil. As such, we refer to our new method as the Aerosol Mineral Fraction (AMF) experiment. Apportionment of emitted silt into the corresponding four size categories transported by the model is prescribed using the fractional size-distribution of surface concentration measured at Tinfou, as in the SMF method.

Finally, for the AMF experiment, we form internal mixtures of minerals with small impurities of iron oxides. These host minerals are important for transporting iron far from its source, because pure iron oxides are more dense and vulnerable to gravitational removal than most minerals comprising dust aerosols. We assume that the mixture of iron oxides within other minerals is smaller where the soil is enriched in total iron oxide, a heuristic attempt to identify regions of enhanced soil weathering that creates pure crystalline iron oxides.

Our AMF model includes an empirical constant γ that controls the amount of aggregation of clay-sized particles in the wet-sieved soil into silt-sized emitted aerosols. We set $\gamma = 2$ for our reference AMF simulation, although we have not made much effort to find an optimal value of this parameter. Results with $\gamma = 0$ are also shown to illustrate the physical origin of the size and regional distributions of minerals within the AMF experiment, and their contrast with respect to the SMF method.

The global emitted mass of particles with diameters less than 32 μm for all experiments is scaled to be identical at 2224 Tg per year. However, in this article, we evaluate the relative proportions of the simulated minerals that are independent of the emission magnitude.

ACPD
15, 3577–3627, 2015

3 Observational data

We compiled measurements of mineral fractions of dust aerosols from almost sixty studies published between the 1960s and the present day that are described in Table 1 and available in Table S1 of the Supplement. Roughly one-third of the studies are in common with a recent compilation focusing on North African sources by Scheuvens et al. (2013). Our compilation includes measurements of mineral fractions of dust concentration and deposition, both from land stations and ship cruises. A few studies provide measurements of dust deposited in permanent snow fields (Windom, 1969; Gaudichet et al., 1992; Zdanowicz et al., 2006). Measurements are not equally distributed over all dust source regions, and mostly sample dust transported from North Africa, the Middle East and Asia (Fig. 1). Only two studies provide measurements downwind of southern African sources (Aston et al., 1973; Chester et al., 1971). No studies were found for dust from North America, while only one site is affected by the Australian dust plume (Windom, 1969). Generally, most of the measurements for aerosol mineral composition are in the Northern Hemisphere and there is underrepresentation of the Southern Hemisphere. Also, many of the measurements in earlier decades were confined to the relative proportions of phyllosilicates.

Methods to determine the mineral composition of dust aerosols have varied over time, and the measurements in our compilation that are based on various instruments and analytical methods contain different biases and uncertainties. Systematic studies of the mineral composition of atmospheric soil dust started in the 1960s, beginning with Delany et al. (1967), who intended to investigate cosmic dust. The mineral composition of airborne dust was usually determined from samples collected on suspended nylon mesh over land or ships (e.g., Prospero and Bonatti, 1969; Goldberg and Griffin, 1970; Parkin et al., 1970; Chester and Johnson, 1971b; Tomadin et al., 1984). Typically, the collection efficiency of the mesh is assumed to be 50 % (Prospero and Bonatti, 1969), but the true value depends upon particle size and wind velocity (Chester and Johnson, 1971a). Parkin et al. (1970) determined a collection efficiency of 100 % for spheri-

ACPD
15, 3577–3627, 2015

cal particles with densities of 3 g cm^{-3} and particle diameters greater than 7 µm, with the efficiency decreasing to 50 % for diameters of 2 µm and null collection of particles with diameters below 0.5 µm. Thus, mesh collection introduces a bias towards larger dust particles, and potentially overestimates the fraction of minerals such as quartz, whose abundance peaks at large particle sizes. Other studies analyzed dust fallen on ship decks (e.g., Game, 1964; Johnson, 1976) or deposited over land (e.g., Goldberg and Griffin, 1970; Tomadin et al., 1984; Khalaf et al., 1985; Adedokum et al., 1989; Skonieczny et al., 2011).

Since the 1990s, airborne dust has been more commonly sampled with other instruments, like high volume air samplers (e.g., Zhou and Tazaki, 1996; Alastuey et al., 2005; Shi et al., 2005; Jeong, 2008; Shen et al., 2009) or low volume air samplers (e.g., Gao and Anderson, 2001; Engelbrecht et al., 2009). These samples extracted dust from the air with polycarbonate or quartz microfibre filters (Shi et al., 2005), cellulose filters (Jeong, 2008), or other filters (Engelbrecht et al., 2009). The finest aerosol particle can get trapped in the quartz fibre filters before the sample is treated for the mineral analysis, a source of collection inefficiency and uncertainty (Alastuey et al., 2005).

The relative mass fractions of the collected minerals are often derived from X-ray diffraction (XRD) spectra (e.g., Prospero and Bonatti, 1969; Alastuey et al., 2005; Shi et al., 2005; Skonieczny et al., 2011). The wavelength of spectral peaks give information about elemental and mineral composition, while the mass fraction relative to other minerals is determined by area under the peak. Characterization of the area of the peak (rather than its maximum) accounts for particle diameters less than 10 µm that cause peak broadening (Glaccum and Prospero, 1980).

XRD analysis is most effective for minerals with a crystal structure whose spectral peaks are well-defined. However, certain minerals like phyllosilicates consist of amorphous material whose orientation can vary from particle to particle, complicating the interpretation of the sample diffraction (Formenti et al., 2008; Kandler et al., 2009). Among the various minerals considered in this study, the fraction of smectite is one of

ACPD
15, 3577–3627, 2015

the most difficult to estimate. Its spectral peaks are small and can lie within the noise level of the XRD analysis (Glaccum and Prospero, 1980). This has been interpreted as the result of low concentration and poor crystallization (Leinen et al., 1994). As a consequence, smectite is occasionally reported only in combination with illite (Shi et al., 2005; Shao et al., 2008). This is additionally due to the frequent interleaving of smectite with illite and other minerals like chlorite, both in soils (Środoń, 1999) and aerosols (Shi et al., 2005; Lu et al., 2006), which can lead to misidentification of the individual phyllosilicates.

The composition of airborne particles is increasingly studied by scanning electron microscope (SEM) images of individual particles along with statistical cluster analysis of elemental composition (e.g., Gao and Anderson, 2001; Lu et al., 2006; Kandler et al., 2009; Engelbrecht et al., 2009).

All the observation data used for our evaluation are based on measurements of the mineral fractions of dust aerosols at the surface. A few studies also provide aircraft measurements (Formenti et al., 2008; Klaver et al., 2011). Those data are not taken into consideration but will be included in future evaluation of simulated vertical profiles.

Because of the difficulty of comparing the uncertainty of different measurement methods, we weight all observations equally. As prognostic models of mineral composition become more common, we hope that mineral attribution of aerosol samples becomes more uniform and routine.

4 Method of evaluation

A major challenge for model evaluation is the difference in record length between climate model output and the mineral observations. Deposition is measured over periods as short as a week. Measurements of surface concentration are based mostly on daily sampling, with reported values from relatively few days. In contrast, the output from our model simulations consists of a continuous stream of data, from which monthly averages are calculated. Note that even though the model output could be archived at

ACPD
15, 3577–3627, 2015

higher frequencies, e.g., every model day, a large discrepancy between the small sample sizes of many of the measurements and large samples from the model simulations would persist. The mineral fractions that we use for evaluation reflect the composition of the soil at the source region. These fractions are probably more consistent than the absolute concentration of the separate minerals used to form this ratio, at least in those remote regions where one a single source dominates the supply. Thus, measurements of mineral fractions from only a few days may be representative of the entire month. Closer to a source, the mineral fractions may be more variable, with episodic increases of quartz and other minerals that are abundant at large diameters during dust storms (cf. Fig. 10 from Kandler et al., 2009). An evaluation of the uncertainty created by the limited measurement duration using daily model output is planned for the future.

For each reference providing measurements, we calculate a time average that can be compared to the model output. In some cases, we estimate a monthly average using daily measurements that are available for only a subset of the month. Our simulations cover only the nine years between 2002 and 2010, but some of the measurements date back to the 1960s. Our evaluation assumes that multi-decadal variability in the mineral fractions of dust aerosols at individual locations is small compared to the fractions themselves. A more thorough discussion of the sampling uncertainty in our comparison between the measurements and model is provided in the Appendix.

We simulate only eight minerals in our model. However, measurements may include additional minerals that are not simulated. Other measurements do not include all of the simulated minerals. (For example, Kandler et al. (2009) does not distinguish smectite from the other phyllosilicates.) To make the measured and simulated mineral fractions comparable, we recalculate the fractions at each individual data point using only minerals present in both the measurements and the model. We caution that this renormalization can be misleading if some minerals that contribute to the total dust mass were simply not reported. (The mineral fraction measurements compiled in Table S1 of the Supplement include all reported minerals, including both those simulated and those omitted from the ModelE.)

ACPD
15, 3577–3627, 2015

To account for different size ranges of the model and measurements, we interpolated the mass fractions from the model size bins to the size range of the measurements. For measurements of total suspended particles (TSP), we compare to the sum over the entire model size range. Since this range extends only to 32 µm, this can lead to a positive bias in the observations for minerals like quartz that are more abundant at larger particle sizes, particularly at measurement locations near dust sources.

We compared the measured and simulated mineral fractions and ratios using scatter plots. We calculate the normalized bias (nBias) and normalized root mean squared error (nRMSE). Normalization was done by dividing the statistic by the average of the observed values used in each scatter plot. The number of paired data points (N) from the measurements and the simulations is also provided with each scatter plot. These summary statistics are computed without weighting: for example, with respect to the number of measurements used to compute the average value of each study. Such precision seems illusory given the incommensurate analytical uncertainty of different measurement types discussed in Sect. 3. Our goal is not to provide a detailed statistical analysis using these metrics but to help identify robust improvement or deterioration of the AMF results compared to the SMF method.

Our evaluation compares measurements from a specific location to the value at the corresponding grid box. In the case of ship cruises, we use the average along the cruise trajectory within each ocean, forming a model average with the corresponding sequence of grid boxes. Our comparison assumes that the grid size of the model is sufficient to resolve spatial variations of the measurements. This is not always the case, particularly near dust sources that are often geographically isolated resulting in strong contrasts of concentration (e.g. Prospero et al., 2002). For example, we discuss below measurements by Engelbrecht et al. (2009) and Al-Dousari and Al-Awadhi (2012), who find large variations in mineral ratios with respect to quartz at nearby locations in the Middle East. Some of these measurements are within a single grid box and thus impossible to resolve with the model.

ACPD
15, 3577–3627, 2015

5 Evaluation of the predicted mineral fractions

In a companion paper (Perlwitz et al., 2015), it is shown that the AMF method brings the model into better agreement with size-resolved measurements of surface concentration at Tinfou, Morroco (Kandler et al., 2009). In contrast to the SMF experiment, the AMF method reproduces the observed large mass fraction of phyllosilicates at silt sizes and reduces the quartz fraction, bringing the latter into agreement with measurements (Fig. 18 in Perlwitz et al., 2015). The AMF method also introduces feldspar and gypsum at clay sizes, despite their exclusion from the MMT and SMF experiment. Both experiments underestimate all mineral fractions at the largest model size category, possibly because the emitted silt is distributed among the corresponding four model size categories using size-resolved measurements of surface concentration as described in Sect. 2.

Below, we extend the evaluation of the size-resolved mineral fractions by both methods to the global scale.

5.1 Seasonal cycle of mineral fractions

Only a few locations have measurements at multiple times throughout the year, although these are generally insufficient to resolve the seasonal cycle. We use these measurements for comparison to the model that at some locations exhibits a seasonal shift in the predominant mineral.

Figure 2 compares the simulated seasonal cycle of the phyllosilicate fraction to measurements at Barbados (Delany et al., 1967) and the Pacific (Leinen et al., 1994; Arnold et al., 1998). The fraction is defined relative to the sum of minerals that are present in both the model and measurements within the same size class. At Barbados, the illite-smectite and kaolinite fractions calculated by the models show contrasting seasonal cycles, driven by the seasonal shift of the Intertropical Convergence Zone (ITCZ) and the Trade Winds over the North Atlantic (Moulin et al., 1997). During summer, dust is preferentially transported from northern African sources enriched in illite and smectite,

ACPD
15, 3577–3627, 2015

in contrast to winter, when dust is emitted from sources farther south containing higher amounts of kaolinite (Caquineau et al., 1998). Both experiments calculate mineral fractions that are consistent with the measurements, although the uncertainty due to the small sample size hampers a robust evaluation.

Over the Pacific, both the SMF and the AMF experiments show similar illite-smectite and kaolinite fractions at clay sizes that are consistent with the observations. The slightly smaller AMF fraction of phyllosilicates results from the addition of feldspar and gypsum at clay sizes that comes at the expense of the phyllosilicate fraction. (This difference between the AMF and SMF treatments of phyllosilicates is obscured in the Barbados measurements, because feldspar and gypsum are not measured and are thus excluded from our reconstruction of the total dust mass at clay sizes.) At silt sizes, the simulated AMF fraction of phyllosilicates that is observed at the Pacific locations is entirely absent in the SMF experiment, highlighting the importance of reconstructing the phyllosilicate mass disaggregated during wet sieving of the soil samples. There is the suggestion that the kaolinite fraction is overestimated by the model at both clay and silt sizes, a discrepancy that is found at other locations, as will be discussed below.

Figure 3 compares the simulated seasonal cycle of feldspar and quartz in the Pacific to ship measurements. Both the AMF and SMF methods predict similar quartz fractions in the clay size range that are close to the observed values. However, the AMF method is in much better agreement with the measurements at silt diameters, whereas the SMF experiment overestimates the quartz fraction by nearly fourfold. Figures 2 and 3 show that the SMF overestimation of the quartz fraction at silt sizes at the expense of phyllosilicates is not limited to Tinfou and more generally, to the vicinity of source regions. The improved agreement of the AMF method results from the reintroduction of phyllosilicate mass into silt sizes through reaggregation, which has the effect of reducing the quartz fraction.

For feldspar, the AMF method reproduces the clay-size fraction of most measurements, in contrast to the SMF experiment which omits feldspar at this size. At silt diam-

ACPD
15, 3577–3627, 2015

eters, both experiments are consistent with the measurements, owing in part to their large uncertainty.

5.2 Global evaluation of mineral fractions

We summarize the model performance by comparison to a global distribution of measurements at silt and clay diameters (Figs. 4 and 5, respectively) as well as its sum over the entire model size range (the “bulk” composition: Fig. 6).

Figure 4 compares the measured and modeled fractions of phyllosilicate and quartz at silt sizes. The measurements cover various regions of the Northern Hemisphere, such as the northern and eastern Pacific (Leinen et al., 1994; Arnold et al., 1998), East Asia (Jeong et al., 2014), the Middle East (Ganor et al., 2000), the eastern Atlantic (Kandler et al., 2007), West Africa (Enete et al., 2012), and northwestern Africa (Kandler et al., 2009). Although there are few measurements restricted to the silt size range (compared to particle mass (PM) measurements that sum all diameters up to a prescribed limit), measurements of these particular minerals are relatively abundant.

At silt diameters, the SMF method systematically overestimates the observed quartz fraction while entirely excluding the phyllosilicates (Fig. 4, top row). As shown previously, this feature is largely corrected by the AMF method (Fig. 4, middle row), as clay-sized soil particles are reaggregated toward silt sizes at the expense of the quartz fraction. The importance of reaggregation to the improved performance of the AMF method is shown by the experiment where the reaggregation parameter γ is set to zero (Fig. 4, bottom row). In the absence of reaggregation, quartz is overestimated and the phyllosilicates are underestimated, replicating the biases of the SMF experiment.

Even with reaggregation, the AMF method tends to underestimate illite at silt sizes, while overestimating kaolinite and smectite (the latter not shown). Combinations of illite with the other phyllosilicates show better agreement. This reveals compensating model biases, although the improved agreement of the combinations may also result from the observational challenge of distinguishing minerals like illite and smectite, and thus the more confident measurement of their combined mass fraction. Figure 5 shows similar biases in the clay-sized fractions of the individual phyllosilicates. The number of phyllosilicate measurements at clay diameters is relatively large, suggesting that these biases are robust. All the experiments have similar biases at clay sizes, suggesting that the error is not the result of reaggregation or the prescribed size distribution of emission within the AMF method. The common biases of the individual phyllosilicates shown in Fig. 5 could result from the MMT that is used to prescribe the clay mineral fractions in all experiments, or the difficulty of distinguishing the individual phyllosilicates during measurement as mentioned above. However, other processes that are not represented in our model could contribute to the bias. For example, we do not represent the preferential gravitational settling and wet removal of smectite during transport that results from its large hygroscopic capacity (Singer et al., 2004), an omission that would contribute to overestimation of this mineral.

Bulk measurements of mineral composition that represent sums over all particle sizes are plentiful compared to measurements within individual size categories. Both the SMF and AMF methods produce similar bulk fractions of phyllosilicates (Fig. 6), with a small negative bias for illite and a positive bias for kaolinite and smectite as previously noted for the individual clay and silt sizes. These biases compensate when the phyllosilicates are considered together (Fig. 6, rightmost column), but the simulated range of fractions remains underestimated by the AMF method.

The nearly uniform simulated fraction of the combined phyllosilicates in the AMF experiment illustrates several potential sources of model error. The error is especially apparent at various locations within the Arabian Peninsula (rightmost column, green points) that are located near dust sources (Al-Dousari and Al-Awadhi, 2012). Many of these measurements are proximal and the large spatial contrasts are difficult to resolve with the model. Moreover, the measured deposition is predominately quartz and carbonate with roughly one-third of the total mass with diameters above 63 µm. Overestimate of the phyllosilicate fraction at these locations could be caused by the model's exclusion of particle diameters above 32 µm that causes the total model dust mass to be underestimated.

ACPD
15, 3577–3627, 2015

Both the SMF and AMF experiments are susceptible to these sources of error, but the latter shows the largest error. The AMF experiment is distinguished by reaggregration, making it especially sensitive to errors in the MMT mineral fractions or the clay-sized fraction of the soil. A more subtle error potentially comes from the apportionment of the emitted silt into the model size bins using observations of surface concentration. We have noted how both experiments underestimate the fraction of every mineral at the largest model silt diameter according to measurements at Tinfou. Correction of this error would reduce the emission of the smaller silt categories (because the apportionment does not change the total silt emission). For the AMF experiment, reduced phyllosilicate emission at the smaller silt sizes would justify increasing our empirical reaggregation parameter to return the model to good agreement with the observations in Fig. 4. That is, the phyllosilicate mass would remain largely unchanged at small silt sizes compared to the present AMF experiment, but emission of all minerals at larger sizes would increase, reducing the fraction of phyllosilicates compared to the total dust mass and bringing it closer to the measured value. A similar redistribution is suggested by measurements of elemental ratios at Tinfou, where potassium increases relative to silicon (Kandler et al., 2009). One interpretation is that feldspar is becoming more important compared to phyllosilicates as their diameters increase. This would result in a distribution of feldspar weighted toward larger silt sizes, in contrast to our current assumption that they share an identical distribution with phyllosilicates. These corrections would have the greatest effect near source regions like the Arabian Peninsula (where the largest particles have not yet been depleted by gravitational settling) and for the AMF experiment, whose fractional emission of total dust at silt sizes is larger than the SMF fraction. The larger point is that near source regions, errors in our apportionment of silt emission have the largest effect, showing the value of size-resolved measurements of emission that distinguish between minerals.

With the exception of source regions and their vicinity, the AMF and SMF methods produce bulk fractions of both total phyllosilicates and quartz that are in good agreement with the measured values (Figs. 6 and 7). This agreement is in spite of clear

ACPD
15, 3577–3627, 2015

biases in the SMF experiment of both mineral fractions at silt sizes (Fig. 4). The SMF method compensates an excessive silt fraction of quartz with smaller silt emission compared to the AMF method. Similarly, the unrealistic restriction of phyllosilicates to clay sizes in the SMF experiments is offset by greater emission at these sizes. Thus, SMF biases within individual size categories are hidden by bulk measurements due to the compensation of these errors.

This compensation is disabled in the AMF experiment with $\gamma = 0$, showing the spurious origin of the agreement of the SMF method with the bulk measurements. For $\gamma = 0$, reaggregation of phyllosilicate mass into the silt category is eliminated, resulting in a quartz fraction identical to the SMF value. However, consistent with the default AMF experiment, fractional emission of clay sizes remains small compared to the SMF experiment in agreement with empirical measurements. As a result, the bulk fraction of phyllosilicates is underestimated for $\gamma = 0$, while there is an overestimate of quartz (Figs. 6 and 7). This shows the compensating effect of enhanced emission of the clay fraction in the SMF experiment that allows good agreement of the total mass, despite biases at silt sizes.

All three experiments show good agreement at the clay-size range for the quartz fraction (Fig. 5). Measurements also show that feldspar is present at this size despite its omission by the SMF method. The clay-sized feldspar in the AMF and AMF ($\gamma = 0$) experiments is constrained by the feldspar content in the silt size range and the observed ratio of emitted silt to clay (Perlwitz et al., 2015, Eq. 14). The lower clay-sized fraction obtained with the AMF method, which is closer to the small amount of observations available, is explained by the reduced mass of silt-sized feldspar in this experiment due to the reaggregation of phyllosilicate mass into the silt-size range.

All the experiments exhibit negative biases for their fractions of carbonates, gypsum, and iron oxide (Fig. 7). These minerals are a relatively small fraction of the soil according to the MMT, and the common model bias suggests that the MMT values may be an underestimate (although the uncertainty of these fractions is large due to limited measurements). The underestimate of iron oxides may result from the exclusion

ACPD
15, 3577–3627, 2015

of goethite by the MMT, a mineral that contributes over half of the measured iron oxide at some locations (Shi et al., 2012; Formenti et al., 2014; Journet et al., 2014). The measurements over the Arabian Peninsula (Al-Dousari and Al-Awadhi, 2012) indicate a negative bias of the carbonate fractions (Fig. 7, green dots), that may result from the model's truncated size range that is a poorer approximation near source regions, as previously discussed.

The figures presented here are constructed from measurements that span either the entire aerosol size range or correspond to a single size category of the MMT. Figure 8 (along with Fig. S1 of the Supplement) compare the model mineral fractions to additional measurements that extend across both MMT size classes. These additional figures support the previous interpretations. However, Fig. 8 shows that all the models consistently overestimate the quartz fraction at PM_{10} (light blue dots). These measurements correspond to the Middle East near source regions (Engelbrecht et al., 2009), and provide additional evidence that the prescribed fractions of emission within the model silt categories are underestimates at the largest sizes with corresponding overestimates at the smaller sizes. This overestimate is consistent with the PM_{10} errors that is largest for the AMF ($\gamma = 0$) experiment that combines the large quartz fraction of the SMF experiment (undiluted by phyllosilicate reaggregation) with the large fraction of emitted silt corresponding to the AMF experiment.

5.3 Ratios of mineral fractions

The mineral fractions with respect to total dust that are analyzed in the previous section avoid the effect of model errors in total emission. For consistency, we have constructed the total dust using only minerals that are common to both the model and the specific measurement study. However, this construction introduces errors where measurements include minerals (within total dust, for example) that are not reported. By considering ratios of specifc pairs of minerals, we avoid this ambiguity, even though distinguishing individual minerals can be more uncertain than measuring the total dust mass.

ACPD
15, 3577–3627, 2015

The identification of quartz is relatively straightforward, and the mineral ratios with respect to quartz are shown in Fig. 9. The figure reiterates model behavior that was illustrated by previous figures of the mineral fraction with respect to the total aerosol mass. For example, in the SMF experiment, phyllosilicates are absent outside of the clay size range, in contradiction to measurements (leftmost column, orange dots). This error is largely fixed in the AMF experiment. This improvement is the result of reaggregation, as shown by the AMF experiment with the reaggregation parameter γ set to zero (bottom row), where the model phyllosilicate fraction is zero at purely silt diameters (orange dots). At clay sizes (dark blue dots), both experiments give similar fractions, reflecting their common derivation from the MMT. Similarly, feldspar and gypsum in the SMF experiment are absent at clay sizes (dark blue dots) as a direct result of the MMT.

Figure 9 shows that all experiments consistently underestimate the range of observed mineral fractions. For every mineral, the largest observed value is greater than the model maximum. The extreme observed values typically correspond to PM_{10} measurements (light blue dots), many derived from the Middle East (Engelbrecht et al., 2009). That the discrepencies are common to all experiments suggests that they do not originate from unique features of each experiment or their treatment of specific minerals other than quartz. The limited horizontal resolution of the model may be one source of error that prevents the reproduction of sharp gradients, especially close to source regions. Alternatively, the underestimated model range may result from the construction of the MMT that is designed to give *mean* mineral fractions that are approximately valid for all examples of a particular arid soil type instead of representing the variations among the examples. Alternatively, the model PM_{10} fractions may be biased by excessive quartz below this diameter. We described above how this might be the result of misapportionment of the emitted silt fraction into the corresponding four size categories that are transported by the model.

Additional ratios with respect to minerals other than quartz are shown in Figs. S3 to S6 of the Supplement.

ACPD
15, 3577–3627, 2015

6 Conclusions

In a companion article (Perlwitz et al., 2015), we define two methods of calculating aerosol mineral composition based upon the Mean Mineralogical Table (MMT) proposed by Claquin et al. (1999). The MMT specifies the mineral composition of both the clay and silt-sized fractions of the soil at each location using a global atlas of arid soil type. For the Soil Mineral Fraction (SMF) method, we assume that the emitted size distribution corresponds to the local soil texture. Both the MMT and soil texture are based upon measurements that follow wet-sieving of the soil sample, whereby soil aggregates are broken into smaller particles. Because the emitted mineral fractions are sensitive to their size distribution within the soil, we define a second experiment called the Aerosol Mineral Fraction (AMF) method that attempts to compensate for this disaggregration by reconstructing the mineral fractions in the original, undisturbed soil that is subject to wind erosion. We propose a simple and approximate reconstruction, where silt-sized aggregrates of phyllosilicates and other minerals are reintroduced at silt sizes in proportion to their abundance at clay sizes in the wet-sieved soil. In addition, we use size-resolved measurements of emission to specify the ratio of emitted clay to silt-sized particles. The emitted clay fraction is observed to be small, so that phyllosilicate aerosols in AMF model originate largely as a result of reaggregation. Because the fraction of emitted silt is fixed, the reintroduction of phyllosilicate aggregates at silt sizes reduces the emitted quartz fraction at this size.

To evaluate the two experiments, we compiled measurements from nearly sixty studies that are distributed both near and far downwind of major dust source regions. In spite of this extensive compilation, many key sources remain undersampled, and insufficient measurements are available to resolve the seasonal cycle of the mineral fractions and corroborate seasonal shifts of the dominant mineral calculated by the model that imply a change in model source region. For example, kaolinite that is abundant in the Sahel dominates model deposition at Barbados during Northern Hemisphere winter, while an increase of emission in North Africa during the summer delivers more illite.

ACPD
15, 3577–3627, 2015

In general, the uneven distribution of measurement sites and their limited duration of operation imposes a large uncertainty that allows us to robustly evaluate only the most general features of the experiments.

Nonetheless, we show that the AMF method addresses key deficiencies of the SMF experiment in comparison to measurements. In particular, AMF phyllosilicates (that are nominally "clay" minerals) are most abundant at silt sizes, while the silt fraction of quartz is reduced compared to the SMF value and closer to measurements. In spite of the more realistic behavior of the AMF method at silt sizes, both experiments show reasonable agreement with the measurements when the entire size range is considered collectively. This is because the emitted clay fraction in the SMF experiment is larger relative to the AMF experiment. This extra emission compensates for the SMF method's absence of silt-sized phyllosilicates. Similarly, the reduced fraction of emission at silt sizes in the SMF experiment compensates for its excessive quartz fraction. The fractional emission of clay and silt sizes in the SMF experiment is based upon the local soil texture and is inconsistent with measurements showing relatively small and regionally invariant emission at clay sizes as assumed by the AMF (e.g Kok, 2011). Thus, measurements of mineral fractions that are sums over all sizes do not distinguish between the AMF and SMF methods because of compensating errors in the latter that are more clearly distinguished by measurements limited to silt diameters. This is shown by a variation of the AMF experiment with reaggregation omitted ($\gamma = 0$). Here, silt-sized phyllosilicates are absent and the quartz fraction is excessive, because the AMF emission at silt sizes is larger than the SMF value.

The AMF method similarly extends feldspar into the clay size range, consistent with measurements. However, the bulk mineral fractions of carbonates, gypsum and iron oxides are underestimated by both methods. The common bias suggests an origin within the MMT fractions. However, the aerosol measurements are infrequent and subject to uncertainty. Another possible reason for underestimate of iron oxide is that the MMT prescribes only hematite, even though goethite is also a source of aerosol iron (Journet et al., 2014).

ACPD
15, 3577–3627, 2015

Both the SMF and AMF experiments reveal a smaller range of mineral ratios compared to the observations. This is possibly a consequence of model resolution that is insufficient to resolve strong contrasts in mineral fractions around isolated source regions. Alternatively, large local variations in the ratio between different minerals may be reduced during construction of the MMT that consists of averages over different examples of the same arid soil type. Common features of the AMF and SMF mineral fractions at clay sizes are a useful test of the MMT, because the emitted fractions in both experiments are unmodified by our method of reaggregation. Recent studies have proposed refinements to the MMT based upon a greater number of soil measurements and inclusion of additional minerals such as chlorite, vermiculite and goethite that are present in measurements (Journet et al., 2014). However, we emphasize that there are other potential sources of model error, including different removal rates resulting from variations of mineral solubility.

We also suggest that several errors may originate from our apportionment of the emitted silt minerals to the transported size bins. We currently use size-resolved measurements of surface concentration of individual minerals at Tinfou, Morocco. However, evaluation of the model mineral fractions suggests that prior deposition has preferentially removed the largest particles (cf. Fig. 18 of Perlwitz et al., 2015), resulting in an underestimate of emission at the largest silt sizes. This corresponds to a compensating overestimate of emission at the smallest silt sizes. This accounts for excessive model values of PM_{10} near source regions, and has implications for the long-range transport of particular minerals like quartz that are typically emitted at larger sizes. This emphasizes the need for size-resolved measurements of emission that distinguish between individual minerals and can replace our current prescription based upon measurements of surface concentration.

Our study is complementary to that of Scanza et al. (2015), who represented brittle fragmentation and reaggregation of the wet-sieved soil to derive the mineral composition of dust aerosols. The improved evaluation of the AMF method in our study in contrast to that of the SMF experiment supports the importance of these processes that modify the mineral fractions of the wet-sieved soil. This shows that these processes need to be included when calculating the climate impact of the individual minerals comprising dust, such as their effect as ice nuclei (Hoose et al., 2008; Atkinson et al., 2013). The improved performance of the AMF method shows that the MMT must be augmented with additional information about the original, undisturbed parent soil subject to wind erosion along with the emission process. The regional distribution of proposed ice nuclei like phyllosilicates and feldspar are very different between the SMF and AMF experiments (cf. Figs. 14 and 15 of Perlwitz et al., 2015), corresponding to a large uncertainty in the impact of these minerals. The limited measurements of aerosol size (that influences global dispersal) are generally insufficient to evaluate the model spatial distribution of the minerals serving as ice nuclei. This is especially true for minerals like feldspar. Moreover, sampling uncertainty of airborne minerals means that the measurements offer only limited guidance to future refinements of the MMT based upon soil analysis. In short, the impacts of dust that depend upon the specific mineral content of the aerosols remain highly uncertain and underconstrained.

Despite the extensive compilation of measurements presented in Table 1, the large remaining uncertainty limits our ability to suggest more precise treatments of aerosol mineral composition and its relation to the compositon of the parent soil. The abundant measurements of bulk mineral fractions far downwind of dust sources are particularly unhelpful to the extent that models can compensate for errors in soil composition through errors in the emitted size fraction. This is important for the transport of iron oxides. Far from the source, crystalline forms of iron have generally been removed as a result of their greater density. The global dispersion of iron oxides is largely as accretions of small impurities upon the surface of other minerals, and is thus tied to the dispersion of these minerals that depends upon their lifetime and thus their size. This shows the value of future measurements of aerosol mineral composition that are size resolved. Currently, these are rare, even though the technology exists for more routine sampling (e.g. Kandler et al., 2009). In contrast, measurements of elemental abundance are relatively ubiquitous and long records exist at stations like Izaña with

ACPD
15, 3577–3627, 2015

relatively little sampling uncertainty (Rodríguez et al., 2011). We will report on an evaluation of the AMF and SMF methods using elemental abundance and the implications for modeling aerosol mineral composition in a subsequent study (Pérez García-Pando et al., 2015).

Appendix A: Sampling uncertainty

We designed the experiments and their evaluation with measurements to emphasize the influence of the calculated aerosol mineral content. For example, we compare mineral fractions rather than the absolute concentration of individual minerals to remove the effect of our uncertainty about the magnitude of global dust emission. Similarly, we relax the model winds toward reanalysis values so that the model mineral fractions are more strongly dependent upon the calculated fractions at emission rather than possible errors in aerosol transport.

Uncertainty of evaluation also results from sampling, including the occasional departure of the measurement duration from the monthly averaging of the model. There are two general cases. In the first case, the measurements represent an average over a duration of a month or longer and can thus be compared directly with the archived model output. The measured quantity in this case is typically deposition. For this example, we calculate the SD of the model, using the nine values available from the nine years simulated by each experiment. The SD allows us to estimate a distribution of possible model values that can be compared to the single measured value. That is, we are asking whether the measured value is consistent with the model distribution. This allows a consistent treatment of measurements that are both within and beyond the range of years corresponding to our experiments. The model mineral fractions are fitted to a beta distribution that is commonly used to represent values that are bounded between zero and one (e.g. Freund, 1992). In the figures, we illustrate the distribution of model values with the 95 % confidence interval of the beta distribution.

In the second case, we have measurements like concentration whose duration is less than the single month used to archive model output. In most examples, we have observations from which we can estimate a time-average for comparison to the model. This average is often over a month, and its uncertainty can be estimated using the standard error $s_{E,O}$:

$$s_{E,O} = \frac{\sigma_O}{\sqrt{N_O}} \tag{A1}$$

where σ_O is the SD of the N_O observations. (For computational convenience, we assume that the observations are distributed normally about their mean rather than according to a beta distribution. Then, the inferred time-average of the observations is within two standard errors of the true value ninety-five percent of the time.) Here, we are essentially using the repeated observations to form a distribution of all possible values during the averaging interval, including those times when measurements were not taken. This distribution is then used to estimate the uncertainty of the mean. In the figures, this uncertainty is represented as two standard errors above and below the inferred time mean.

There are a few examples where daily measurements (or more generally, measurements over sub-monthly durations) are scattered over a much longer period. In some cases, the precise date of measurement is unknown (e.g. Engelbrecht et al., 2009). In these cases, the uncertainty of the corresponding time average is probably bounded by the annual cycle that we estimate using the SD of the measurements. Our uncertainty estimate is not particularly precise, but fortunately, there are relatively few cases of this type.

A more rare case is where we have a measurement for only a single day (e.g. Alastuey et al., 2005). Here we compare this single measurement directly to the monthly average of the model. We estimate the uncertainty of the single measurement as a monthly average by borrowing its SD from that calculated using the model. We cannot directly calculate the daily SD from model output, but we make the assumption

ACPD
15, 3577–3627, 2015

that interannual variations in the model monthly means result solely from averaging over sub-monthly fluctuations. Then, we can estimate σ_M, the model SD at the time scale of the observation interval ΔT_O (one day, in this example) according to:

$$\sigma_M = \sqrt{\frac{N_M}{\Delta T_O}}\sigma_{M,\mathrm{monthly}}, \tag{A2}$$

where $\sigma_{M,\mathrm{monthly}}$ is the interannual SD of the monthly averages, and N_M represents the number of days in the month corresponding to the measurement. In the figure, the uncertainty is illustrated as two SDs above and below the single observed value.

There are a number of assumptions that go into our calculation of measurement uncertainty. For example, Eq. (A1) assumes that successive measurements are not correlated. It is straightforward to replace the number of observations with an effective number if the data show that autocorrelation cannot be neglected. In addition, the calculation of the sub-monthly SD in terms of interannual variability according to Eq. (A2) assumes that fluctuations of the mineral fractions have uniform spectral power at periods longer than the sub-monthly measurement interval. In general, our less defensible assumptions are necessitated by the sparse measurement record. This shows the urgent value of future measurements of aerosol mineral composition that are widespread and routine that would reduce the need for imprecise and heuristic characterizations of uncertainty like Eq. (A2). In any case, the conclusions we draw from this study are based upon differences between the experiments that are qualitatively apparent and that do not rely upon intricate statistical analysis.

The Supplement related to this article is available online at doi:10.5194/acpd-15-3577-2015-supplement.

ACPD
15, 3577–3627, 2015

Acknowledgements. We thank Paul Ginoux, Konrad Kandler, Natalie Mahowald, Sergio Rodríguez and Rachel Scanza for helpful conversations. This research was supported by the National Science Foundation (ATM-01-24258), the Department of Energy (DE-SC0006713), the NASA Modeling, Analysis and Prediction Program and the Ministry of Economy and Competitiveness of Spain through the POLLINDUST (CGL2011-26259). Computational resources were provided by the NASA High-End Computing (HEC) Program through the NASA Center for Climate Simulation (NCCS) at Goddard Space Flight Center.

References

Adedokum, J. A., Emofurieta, W. O., and Adedeji, O. A.: Physical, mineralogical and chemical properties of harmattan dust at Ile-Ife, Nigeria, Theor. Appl. Climatol., 40, 161–169, doi:10.1007/BF00866179, 1989. 3585, 3614

Al-Awadhi, J. M. and AlShuaibi, A. A.: Dust fallout in Kuwait city: deposition and characterization, Sci. Total Environ., 461–462, 139–148, doi:10.1016/j.scitotenv.2013.03.052, 2013. 3614

Al-Dousari, A. M. and Al-Awadhi, J.: Dust fallout in Northern Kuwait, major sources and characteristics, Kuwait J. Sci. Eng., 39, 171–187, 2012. 3588, 3592, 3595, 3614

Al-Dousari, A. M., Al-Awadhi, J., and Ahmed, M.: Dust fallout characteristics within global dust storm major trajectories, Arab. J. Geosci., 6, 3877–3884, doi:10.1007/s12517-012-0644-0, 2013. 3614

Alastuey, A., Querol, X., Castillo, S., Escudero, M., Avila, A., Cuevas, E., Torres, C., Romero, P.-M., Exposito, F., García, O., Diaz, J. P., Van Dingenen, R., and Putaud, J. P.: Characterisation of TSP and $PM_{2.5}$ at Izaña and Sta. Cruz de Tenerife (Canary Islands, Spain) during a Saharan Dust Episode (July 2002), Atmos. Environ., 39, 4715–4728, doi:10.1016/j.atmosenv.2005.04.018, 2005. 3585, 3602, 3614

Arnold, E., Merrill, J., Leinen, M., and King, J.: The effect of source area and atmospheric transport on mineral aerosol collected over the North Pacific Ocean, Global Planet. Change, 18, 137–159, doi:10.1016/S0921-8181(98)00013-7, 1998. 3589, 3591, 3614

Aston, S. R., Chester, R., Johnson, L. R., and Padgham, R. C.: Eolian dust from the lower atmosphere of the Eastern Atlantic and Indian Oceans, China Sea and Sea of Japan, Mar. Geol., 14, 15–28, doi:10.1016/0025-3227(73)90040-6, 1973. 3584, 3614

Atkinson, J. D., Murray, B. J., Woodhouse, M. T., Whale, T. F., Baustian, K. J., Carslaw, K. S., Dobbie, S., O'Sullivan, D., and Malkin, T. L.: The importance of feldspar for ice nucleation by mineral dust in mixed-phase clouds, Nature, 498, 355–358, doi:10.1038/nature12278, 2013. 3579, 3600

Avila, A., Queralt-Mitjans, I., and Alarcón, M.: Mineralogical composition of African dust delivered by red rains over northeastern Spain, J. Geophys. Res., 102, 21977–21996, doi:10.1029/97JD00485, 1997. 3614

Awadh, S. M.: Geochemistry and mineralogical composition of the airborne particles of sand dunes and dust storms settled in Iraq and their environmental impact, Environ. Earth. Sci., 66, 2247–2256, doi:10.1007/s12665-011-1445-6, 2012. 3614

Caquineau, S., Gaudichet, A., Gomes, L., Magonthier, M., and Chatenet, B.: Saharan dust: clay ratio as a relevant tracer to assess the origin of soil derived aerosols, Geophys. Res. Lett., 25, 983–986, doi:10.1029/98GL00569, 1998. 3590

Chester, R. and Johnson, L. R.: Atmospheric dusts collected off the Atlantic coast of North Africa and the Iberian Peninsula, Mar. Geol., 11, 251–260, doi:10.1016/0025-3227(71)90027-2, 1971a. 3584, 3614

Chester, R. and Johnson, L. R.: Atmospheric dust collected off the West African Coast, Nature, 229, 105–107, doi:10.1038/229105b0, 1971b. 3584, 3614

Chester, R., Elderfield, H., and Griffin, J. J.: Dust transported in the North-east and South-east Trade Winds in the Atlantic Ocean, Nature, 233, 474–476, doi:10.1038/233474a0, 1971. 3584, 3614

Chester, R., Elderfield, H., Griffin, J. J., Johnson, L., and Padgham, R. C.: Eolian dust along the eastern margins of the Atlantic Ocean, Mar. Geol., 13, 91–105, doi:10.1016/0025-3227(72)90048-5, 1972. 3614

Chester, R., Baxter, G. G., Behairy, A. K. A., Connor, K., Cross, D., Elderfield, H., and Padgham, R. C.: Soil-sized eolian dusts from the lower troposphere of the eastern Mediterranean Sea, Mar. Geol., 24, 201–217, doi:10.1016/0025-3227(77)90028-7, 1977. 3615

Chester, R., Sharples, E. J., Sanders, G. S., and Saydam, A. C.: Saharan dust incursion over the Tyrrhenian Sea, Atmos. Environ., 18, 929–935, doi:10.1016/0004-6981(84)90069-6, 1984. 3615

Choate, L. M., Ranville, J. F., Bunge, A. L., and Macalady, D. L.: Dermally adhered soil: 2. Reconstruction of dry-sieve particle-size distributions from wet-sieve data, Integrated Envi-

ronmental Assessment and Management, 2, 385–390, doi:10.1002/ieam.5630020410, 2006. 3579
Claquin, T., Schulz, M., and Balkanski, Y. J.: Modeling the mineralogy of atmospheric dust sources, J. Geophys. Res., 104, 22,243–22,256, doi:10.1029/1999JD900416, 1999. 3579, 3580, 3581, 3582, 3597
Delany, A. C., Delany, A. C., Parkin, D. W., Griffin, J. J., Goldberg, E. D., and Reimann, B. E. F.: Airborne dust collected at Barbados, Geochim. Cosmochim. Ac., 31, 885–909, doi:10.1016/S0016-7037(67)80037-1, 1967. 3584, 3589, 3615
Díaz-Hernández, J. L., Martín-Ramos, J. D., and Lez-Galindo, A.: Quantitative analysis of mineral phases in atmospheric dust deposited in the south-eastern Iberian Peninsula, Atmos. Environ., 45, 3015–3024, doi:10.1016/j.atmosenv.2011.03.024, 2011. 3615
Enete, I. C., Obienusi, E. A., Igu, I. N., and Ayadiulo, R.: Harmattan dust: composition, characteristics and effects on soil fertility in Enugu, Nigeria, British Journal of Applied Science & Technology, 2, 72–81, doi:10.9734/BJAST/2012/950, 2012. 3591, 3615
Engelbrecht, J. P., McDonald, E. V., Gillies, J. A., Jayanty, R. K. M., Casuccio, G., and Gertler, A. W.: Characterizing mineral dusts and other aerosols from the Middle East Part 1: Ambient sampling, Inhal. Toxicol., 21, 297–326, doi:10.1080/08958370802464273, 2009. 3585, 3586, 3588, 3595, 3596, 3602, 3615
Engelbrecht, J. P., Menéndez, I., and Derbyshire, E.: Sources of $PM_{2.5}$ impacting on Gran Canaria, Spain, Catena, 117, 119–132, doi:10.1016/j.catena.2013.06.017, 2014. 3615
Falkovich, A. H., Ganor, E., Levin, Z., Formenti, P., and Rudich, Y.: Chemical and mineralogical analysis of individual mineral dust particles, J. Geophys. Res., 106, 18029–18036, doi:10.1029/2000JD900430, 2001. 3615
FAO: Digital Soil Map of the World, Food and Agriculture Organization, Rome, Italy, 2007. 3579
FAO/IIASA/ISRIC/ISSCAS/JRC: Harmonized World Soil Database (version 1.2), FAO, Rome, Italy and IIASA, Laxenburg, Austria, available at: http://webarchive.iiasa.ac.at/Research/LUC/External-World-soil-database/HTML/HWSD_Data.html?sb=4, 2012. 3579
Ferguson, W. S., Griffin, J. J., and Goldberg, E. D.: Atmospheric dust from the North Pacific – a short note on a long range eolian transport, J. Geophys. Res., 75, 1137–1139, doi:10.1029/JC075i006p01137, 1970. 3615
Fiol, L. A., Fornós, J. J., Gelabert, B., and Guijarro, J. A.: Dust rains in Mallorca (Western Mediterranean): their occurrence and role in some recent geological processes, Catena, 63, 64–84, doi:10.1016/j.catena.2005.06.012, 2005. 3615

ACPD
15, 3577–3627, 2015

Formenti, P., Rajot, J. L., Desboeufs, K., Caquineau, S., Chevaillier, S., Nava, S., Gaudichet, A., Journet, E., Triquet, S., Alfaro, S., Chiari, M., Haywood, J., Coe, H., , and Highwood, E.: Regional variability of the composition of mineral dust from western Africa: results from the AMMA SOP0/DABEX and DODO field campaigns, J. Geophys. Res., 113, D00C13, doi:10.1029/2008JD009903, 2008. 3585, 3586, 3615

Formenti, P., Caquineau, S., Chevaillier, S., Klaver, A., Desboeufs, K., Rajot, J. L., Belin, S., and Briois, V.: Dominance of goethite over hematite in iron oxides of mineral dust from Western Africa: quantitative partitioning by X-ray absorption spectroscopy, J. Geophys. Res., 119, 12740–12754, doi:10.1002/2014JD021668, 2014. 3595

Freund, J. E.: Mathematical Statistics, 5th edn., Prentice Hall, Inc., Englewood Cliffs, New Jersey, 1992. 3601

Game, P. M.: Observations on a dustfall in the Eastern Atlantic, February, 1962, J. Sediment. Petrol., 34, 355–359, doi:10.1306/74D7105F-2B21-11D7-8648000102C1865D, 1964. 3585, 3615

Ganor, E.: The composition of clay minerals transported to Israel as indicators of Saharan dust emission, Atmos. Environ., 25, 2657–2664, doi:10.1016/0960-1686(91)90195-D, 1991. 3615

Ganor, E., Deutsch, Y., and Foner, H. A.: Mineralogical composition and sources of airborne settling particles on Lake Kinneret (the Sea of Galilee), Israel, Water Air Soil Poll., 118, 245–262, doi:10.1023/A:1005167230795, 2000. 3591, 3615

Gao, Y. and Anderson, J. R.: Characteristics of Chinese aerosols determined by individual-particle analysis, J. Geophys. Res., 106, 18037–18045, doi:10.1029/2000JD900725, 2001. 3585, 3586

Gaudichet, A., Lefèvre, R., Gaudry, A., Ardouin, B., Lambert, G., and Miller, J. M.: Mineralogical composition of aerosols at Amsterdam Island, Tellus, 41, 344–352, doi:10.1111/j.1600-0889.1989.tb00313.x, 1989. 3615

Gaudichet, A., Angclis, M. D., Joussaume, S., Petit, J. R., Korotkevitch, Y. S., and Petrov, V. N.: Comments on the origin of dust in East Antarctica for present and ice-age conditions, J. Atmos. Chem., 14, 192–142, doi:10.1007/BF00115229, 1992. 3584, 3616

Gillette, D. A., Blifford Jr., I. H., and Fryrear, D. W.: The influence of wind velocity on the size distributions of aerosols generated by the wind erosion of soils, J. Geophys. Res., 79, 4068–4075, doi:10.1029/JC079i027p04068, 1974. 3583

ACPD
15, 3577–3627, 2015

Glaccum, R. A. and Prospero, J. M.: Saharan aerosols over the tropical North Atlantic Mineralogy, Mar. Geol., 37, 295–321, doi:10.1016/0025-3227(80)90107-3, 1980. 3585, 3586, 3616

Goldberg, E. D. and Griffin, J. J.: The sediments of the Northern Indian Ocean, Deep-Sea Res., 17, 513–537, doi:10.1016/0011-7471(70)90065-3, 1970. 3584, 3585, 3616

Hoose, C., Lohmann, U., Erdin, R., and Tegen, I.: The global influence of dust mineralogical composition on heterogeneous ice nucleation in mixed-phase clouds, Environ. Res. Lett., 3, 025003, doi:10.1088/1748-9326/3/2/025003, 2008. 3579, 3600

Jeong, G. Y.: Bulk and single-particle mineralogy of Asian dust and a comparison with its source soils, J. Geophys. Res., 113, D02208, doi:10.1029/2007JD008606, 2008. 3585, 3616

Jeong, G. Y. and Achterberg, E. P.: Chemistry and mineralogy of clay minerals in Asian and Saharan dusts and the implications for iron supply to the oceans, Atmos. Chem. Phys., 14, 12415–12428, doi:10.5194/acp-14-12415-2014, 2014. 3616

Jeong, G. Y., Kim, J. Y., Seo, J., Kim, G. M., Jin, H. C., and Chun, Y.: Long-range transport of giant particles in Asian dust identified by physical, mineralogical, and meteorological analysis, Atmos. Chem. Phys., 14, 505–521, doi:10.5194/acp-14-505-2014, 2014. 3591, 3616

Johnson, L. R.: Particle-size fractionation of eolian dust during transport and sampling, Mar. Geol., 21, M17–M21, doi:10.1016/0025-3227(76)90099-2, 1976. 3585, 3616

Journet, E., Balkanski, Y., and Harrison, S. P.: A new data set of soil mineralogy for dust-cycle modeling, Atmos. Chem. Phys., 14, 3801–3816, doi:10.5194/acp-14-3801-2014, 2014. 3579, 3595, 3598, 3599

Kalnay, E., Kanamitsu, M., Kistler, R., Collins, W., Deaven, D., Gandin, L., Iredell, M., Saha, S., White, G., Woollen, J., Zhu, Y., Leetmaa, A., Reynolds, R., Chelliah, M., Ebisuzaki, W., Higgins, W., Janowiak, J., Mo, K. C., Ropelewski, C., Wang, J., Jenne, R., and Joseph, D.: The NCEP/NCAR 40-year reanalysis project, B. Am. Meteorol. Soc., 77, 437–471, doi:10.1175/1520-0477(1996)077<0437:TNYRP>2.0.CO;2, 1996. 3581

Kandler, K., Benker, N., Bundke, U., Cuevas, E., Ebert, M., Knippertz, P., Rodríguez, S., Schütz, L., and Weinbruch, S.: Chemical composition and complex refractive index of Saharan Mineral Dust at Izaña, Tenerife (Spain) derived by electron microscopy, Atmos. Environ., 41, 8058–8074, doi:10.1016/j.atmosenv.2007.06.047, 2007. 3591, 3616

Kandler, K., Schütz, L., Deutscher, C., Ebert, M., Hofmann, H., Jäckel, S., Jaenicke, R., Knippertz, P., Lieke, K., Massling, A., Petzold, A., Schladitz, A., Weinzierl, B., Wiedensohler, A., Zorn, S., and Weinbruch, S.: Size distribution, mass concentration, chemical and mineralog-

ACPD

15, 3577–3627, 2015

ical composition and derived optical parameters of the boundary layer aerosol at Tinfou, Morocco, during SAMUM 2006, Tellus B, 61, 32–50, doi:10.1111/j.1600-0889.2008.00385.x, 2009. 3582, 3585, 3586, 3587, 3589, 3591, 3593, 3600, 3616

Kandler, K., Schütz, L., Jäckel, S., Lieke, K., Emmel, C., Müller-Ebert, D., Ebert, M., Scheuvens, D., Schladitz, A., Šegvić, B., Wiedensohler, A., and Weinbruch, S.: Ground-based off-line aerosol measurements at Praia, Cape Verde, during the Saharan Mineral Dust Experiment: microphysical properties and mineralogy, Tellus B, 63, 459–474, doi:10.1111/j.1600-0889.2011.00550.x, 2011. 3617

Khalaf, F. I., Al-Kadi, A., and Al-Saleh, S.: Mineralogical composition and potential sources of dust fallout deposits in Kuwait, northern Arabian Gulf, Sediment. Geol., 42, 255–278, doi:10.1016/0037-0738(85)90047-8, 1985. 3585, 3617

Klaver, A., Formenti, P., Caquineau, S., Chevaillier, S., Ausset, P., Calzolai, G., Osborne, S., Johnson, B., Harrison, M., and Dubovik, O.: Physico-chemical and optical properties of Sahelian and Saharan mineral dust: in situ measurements during the GERBILS campaign, Q. J. Roy. Meteor. Soc., 137, 1193–1210, doi:10.1002/qj.889, 2011. 3586

Kok, J. F.: A scaling theory for the size distribution of emitted dust aerosols suggests climate models underestimate the size of the global dust cycle, P. Natl. Acad. Sci. USA, 108, 1016–1021, doi:10.1073/pnas.1014798108, 2011. 3583, 3598

Laurent, B., Marticorena, B., Bergametti, G., Léon, J. F., and Mahowald, N. M.: Modeling mineral dust emissions from the Sahara desert using new surface properties and soil database, J. Geophys. Res.-Atmos., 113, D14218, doi:10.1029/2007JD009484, 2008. 3579

Leinen, M., Prospero, J. M., Arnold, E., and Blank, M.: Mineralogy of aeolian dust reaching the North Pacific Ocean 1. Sampling and analysis, J. Geophys. Res., 99, 21017–21023, doi:10.1029/94JD01735, 1994. 3586, 3589, 3591, 3617

Lu, S., Shao, L., Wu, M., and Jiao, Z.: Mineralogical characterization of airborne individual particulates in Bejing PM_{10}, J. Environ. Sci., 18, 90–95, available at: http://iospress.metapress.com/content/52ganfy7xb25a0ma/, 2006. 3586, 3617

Menéndez, I., Díaz-Hernández, J. L., Mangas, J., Alonso, I., and Sánchez-Soto, P. J.: Airborne dust accumulation and soil development in the North-East sector of Gran Canaria (Canary Islands, Spain), J. Arid Environ., 71, 57–81, doi:10.1016/j.jaridenv.2007.03.011, 2007. 3617

Møberg, J. P., Esu, I. E., and Malgwi, W. B.: Characteristics and constituent composition of Harmattan dust falling in Northern Nigeria, Geoderma, 48, 73–81, doi:10.1016/0016-7061(91)90007-G, 1991. 3617

ACPD
15, 3577–3627, 2015

Moulin, C., Lambert, C. E., Dulac, F., and Dayan, U.: Control of atmospheric export of dust from North Africa by the North Atlantic Oscillation, Nature, 387, 691–694, available at: http://www.nature.com/nature/journal/v387/n6634/full/387691a0.html, 1997. 3589

Nickovic, S., Vukovic, A., Vujadinovic, M., Djurdjevic, V., and Pejanovic, G.: Technical Note: High-resolution mineralogical database of dust-productive soils for atmospheric dust modeling, Atmos. Chem. Phys., 12, 845–855, doi:10.5194/acp-12-845-2012, 2012. 3579, 3581

O'Hara, S. L., Clarke, M. L., and Elatrash, M. S.: Field measurements of desert dust deposition in Libya, Atmos. Environ., 40, 3881–3897, doi:10.1016/j.atmosenv.2006.02.020, 2006. 3617

Parkin, D. W., Phillips, D. R., Sullivan, R. A. L., and Johnson, L.: Airborne dust collections over the North Atlantic, J. Geophys. Res., 75, 1782–1793, doi:10.1029/JC075i009p01782, 1970. 3584, 3617

Parkin, D. W., Phillips, D. R., Sullivan, R., and Johnson, L.: Airborne dust collections down the Atlantic, Q. J. Roy. Meteor. Soc., 98, 798–808, doi:10.1002/qj.49709841807, 1972. 3617

Pérez García-Pando, C., Perlwitz, J. P., Miller, R. L., and Rodriguez, S.: Dust elemental composition at Izaña Observatory: modeling and observations, in preparation, 2015. 3580, 3601

Perlwitz, J. P., Pérez García-Pando, C., and Miller, R. L.: Predicting the mineral composition of dust aerosols – Part 1: Representing key processes, Atmos. Chem. Phys. Discuss., 15, 3493–3575, doi:10.5194/acpd-15-3493-2015, 2015. 3579, 3580, 3581, 3582, 3589, 3594, 3597, 3599, 3600

Prospero, J. M. and Bonatti, E.: Continental dust in the atmosphere of the Eastern Equatorial Pacific, J. Geophys. Res., 74, 3362–3371, doi:10.1029/JC074i013p03362, 1969. 3584, 3585, 3617

Prospero, J. M., Glaccum, R. A., and Nees, R. T.: Atmospheric transport of soil dust from Africa to South America, Nature, 289, 570–572, doi:10.1038/289570a0, 1981. 3617

Prospero, J. M., Ginoux, P., Torres, O., Nicholson, S. E., and Gill, T. E.: Environmental characterization of global sources of atmospheric soil dust identified with the Nimbus 7 Total Ozone Mapping Spectrometer (TOMS) absorbing aerosol product, Rev. Geophys., 40, 2-1–2-31, doi:10.1029/2000RG000095, 2002. 3588

Queralt-Mitjans, I., Domingo, F., and Sole-Benet, A.: The influence of local sources on the mineral content of bulk deposition over an altitudinal gradient in the Filabres Range (SE Spain), J. Geop, 98, 16761–16768, doi:10.1029/93JD01281, 1993. 3617

Rashki, A., Eriksson, P. G., de W. Rautenbach, C. J., Kaskaoutis, D. G., Grote, W., and Dykstra, J.: Assessment of chemical and mineralogical characteristics of airborne dust in the

Sistan region, Iran, Chemosphere, 90, 227–236, doi:10.1016/j.chemosphere.2012.06.059, 2013. 3617

Rayner, N. A., Parker, D. E., Horton, E. B., Folland, C. K., Alexander, L. V., Rowell, D. P., Kent, E. C., and Kaplan, A.: Global analyses of sea surface temperature, sea ice, and night marine air temperature since the late nineteenth century, J. Geophys. Res., 108, 4407, doi:10.1029/2002JD002670, 2003. 3581

Rodríguez, S., Alastuey, A., Alonso-Pérez, S., Querol, X., Cuevas, E., Abreu-Afonso, J., Viana, M., Pérez, N., Pandolfi, M., and de la Rosa, J.: Transport of desert dust mixed with North African industrial pollutants in the subtropical Saharan Air Layer, Atmos. Chem. Phys., 11, 6663–6685, doi:10.5194/acp-11-6663-2011, 2011. 3601

Scanza, R. A., Mahowald, N., Ghan, S., Zender, C. S., Kok, J. F., Liu, X., Zhang, Y., and Albani, S.: Modeling dust as component minerals in the Community Atmosphere Model: development of framework and impact on radiative forcing, Atmos. Chem. Phys., 15, 537–561, doi:10.5194/acp-15-537-2015, 2015. 3599

Scheuvens, D. and Kandler, K.: On composition, morphology, and size distribution of airborne mineral dust, in: Mineral Dust: A Key Player in the Earth System, chap. 2, edited by: Knippertz, P. and Stuut, J.-B., Springer Netherlands, Dordrecht Heidelberg New York London, doi:10.1007/978-94-017-8978-3_2, 15–49, 2014. 3579

Scheuvens, D., Schütz, L., Kandler, K., Ebert, M., and Weinbruch, S.: Bulk composition of northern African dust and its source sediments and its source sediments – a compilation, Earth-Sci. Rev., 116, 170–194, doi:10.1016/j.earscirev.2012.08.005, 2013. 3584

Shao, L., Li, W., Xiao, Z., and Sun, Z.: The mineralogy and possible sources of spring dust particles over Bejing, Adv. Atmos. Sci., 25, 395–403, doi:10.1007/s00376-008-0395-8, 2008. 3586, 3617

Shao, Y.: A model for mineral dust emission, J. Geophys. Res., 106, 20239–20254, doi:10.1029/2001JD900171, 2001. 3579

Shen, Z., Cao, J., Li, X., Okuda, T., Wang, Y., and Wang, X.: Mass concentration and mineralogical characteristics of aerosol particles collected at Dunhuang during ACE-Asia, Adv. Atmos. Sci., 23, 291–298, doi:10.1007/s00376-006-0291-z, 2006. 3617

Shen, Z., Caquineau, S., Cao, J., Zhang, X., Han, Y., Gaudichet, A., and Gomes, L.: Mineralogical characteristics of soil dust from source regions in northern China, Particuology, 7, 507–512, doi:10.1016/j.partic.2009.10.001, 2009. 3585, 3617

Shi, Z., Shao, L., Jones, T. P., and Lu, S.: Microscopy and mineralogy of airborne particles collected during severe dust storm episodes in Beijing, China, J. Geophys. Res., 110, D01303, doi:10.1029/2004JD005073, 2005. 3585, 3586, 3618

Shi, Z., Krom, M. D., Jickells, T. D., Bonneville, S., Carslaw, K. S., Mihalopoulos, N., Baker, A. R., and Benning, L. G.: Impacts on iron solubility in the mineral dust by processes in the source region and the atmosphere: a review, Aeolian Research, 5, 21–42, doi:10.1016/j.aeolia.2012.03.001, 2012. 3595

Singer, A., Dultz, S., and Argaman, E.: Properties of the non-soluble fractions of suspended dust over the Dead Sea, Atmos. Environ., 38, 1745–1753, doi:10.1016/j.atmosenv.2003.12.026, 2004. 3592

Skonieczny, C., Bory, A., Bout Roumazeilles, V., Abouchami, W., Galer, S. J. G., Crosta, X., Stuut, J., Meyer, I., Chiapello, I., Podvin, T., Chatenet, B., Diallo, A., and Ndiaye, T.: The 713 March 2006 major Saharan outbreak: multiproxy characterization of mineral dust deposited on the West African margin, J. Geophys. Res., 116, D18210, doi:10.1029/2011JD016173, 2011. 3585

Skonieczny, C., Bory, A., Bout-Roumazeilles, V., Abouchami, W., Galer, S. J. G., Crosta, X., Diallo, A., and Ndiaye, T.: A three-year time series of mineral dust deposits on the West African margin: Sedimentological and geochemical signatures and implications for interpretation of marine paleo-dust records, Earth Planet. Sc. Lett., 364, 145–156, doi:10.1016/j.epsl.2012.12.039, 2013. 3618

Sow, M., Alfaro, S. C., Rajot, J. L., and Marticorena, B.: Size resolved dust emission fluxes measured in Niger during 3 dust storms of the AMMA experiment, Atmos. Chem. Phys., 9, 3881–3891, doi:10.5194/acp-9-3881-2009, 2009. 3583

Środoń, J.: Nature of mixed-layer clays and mechanisms of their formation and alteration, Annu. Rev. Earth Pl. Sc., 27, 19–53, doi:10.1146/annurev.earth.27.1.19, 1999. 3586

Tomadin, L., Lenaz, R., Landuzzi, V., Mazzucotelli, A., and Vannucci, R.: Wind-blown dust over the Central Mediterranean, Oceanol. Acta, 7, 13–23, 1984. 3584, 3585, 3618

Windom, H. L.: Atmospheric dust records in permanent snowfields: implications to marine sedimentation, Geol. Soc. Am. Bull., 80, 761–782, doi:10.1130/0016-7606(1969)80[761:ADRIPS]2.0.CO;2, 1969. 3584, 3618

Zdanowicz, C., Hall, G., Vaive, J., Amelin, Y., Percival, J., Girard, I., Biscaye, P., and Bory, A.: Asian dustfall in the St. Elias Mountains, Yukon, Canada, Geochim. Cosmochim. Ac., 70, 3493–3507, doi:10.1016/j.gca.2006.05.005, 2006. 3584, 3618

ACPD
15, 3577–3627, 2015

Predicting the mineral composition of dust aerosols – Part 2

J. P. Perlwitz et al.

Zhou, G. and Tazaki, K.: Seasonal variation of gypsum in aerosol and its effect on the acidity of wet precipitation on the Japan Sea side of Japan, Atmos. Environ., 30, 3301–3308, doi:10.1016/1352-2310(96)00071-4, 1996. 3585, 3618

ACPD
15, 3577–3627, 2015

Predicting the mineral composition of dust aerosols – Part 2

J. P. Perlwitz et al.

Table 1. List of literature references for mineral fraction measurements (predicted with ModelE: M – mica/illite/muscovite, K – kaolinite, S – smectite, C – carbonates, Q – quartz, F – feldspar, I – iron oxides, G – gypsum; not predicted other minerals: O) with specific information about months of measurements with size range, geographical coordinates, and time range of measurements.

Reference	Minerals	Size Range	Location	Time Range
Adedokum et al. (1989)	M K Q F O	Total	Ile-Ife, Nigeria	01–02/1984, 01–02/1985
Alastuey et al. (2005)	M K C Q F G O	Total	Izaña and Sta. Cruz de Tenerife, Canary Islands, Spain	07/29/2002
Al-Awadhi and AlShuaibi (2013)	M C Q F O	Total	10 sites in Kuwait City, Kuwait	03/2011–02/2012 (monthly)
Al-Dousari and Al-Awadhi (2012)	M + K + S C Q F O	Total	10 locations in Arabian Peninsula	11/2006–12/2007 (monthly)
Al-Dousari et al. (2013)	M + K + S C Q F O	Total	11 global locations	01/2007–12/2007 (monthly)
Arnold et al. (1998)	M K S Q F O	< 2 µm; 2–20 µm	1: North of Hawaii 2: Northeast Pacific	1: 05/1986 2: 03–04/1987
Aston et al. (1973)	1:M K S O; 2:C Q O	1:< 2 µm; 2: Total	Eastern North and South Atlantic, Indian Ocean, Sea of China	07/1971–11/1971
Avila et al. (1997) [a]	M K S C Q F O	Total	Montseny Mountains, Spain	11/1984–03/1992
Awadh (2012)	C Q F G O	Total	Baghdad, Iraq	03/2008–06/2008
Chester and Johnson (1971a)	M K S O	< 2 µm	Eastern Atlantic	11/06/1970–11/13/1970
Chester and Johnson (1971b)	M K S O	< 2 µm	Eastern Atlantic	04/22/1969–05/05/1969
Chester et al. (1971)	M K S O	< 2 µm	Eastern Atlantic	07/1970–08/1970
Chester et al. (1972)	M K S O	< 2 µm	Eastern Atlantic	03/17/1971–03/28/1971

ACPD
15, 3577–3627, 2015

Table 1. Continued.

Reference	Minerals	Size Range	Location	Time Range
Chester et al. (1977)	1:M K S O 2:Q C	1:< 2 µm 2: Total	Eastern Mediterranean	Summer 1972, Spring 1975
Chester et al. (1984)	M K S O	< 2 µm	Tyrrhenian Sea	10/08/1979– 10/25/1979
Delany et al. (1967)	M K S Q O	< 2 µm	Barbados	10/1965–01/1966
Díaz-Hernández et al. (2011)	M K S C Q F G O	Total	Granada Depression, Spain	1992
Enete et al. (2012)	1:M K Q F 2:M K Q F I O	1:< 2 µm 2: 2–50 µm	2 sites in Enugu, Nigeria	10/2009–04/2010, 10/2010–04/2011 (weekly)
Engelbrecht et al. (2009)	M + K + S[b] C Q F I O	< 10 µm	14 site in Central and West Asia and 1 site in Djibouti	2005 to 2007
Engelbrecht et al. (2014)	M + K + S[b] C Q I[c] G O	< 2.5 µm	Las Palmas de Gran Canaria, Spain	01/12/2010– 11/27/2010 (2 to 13 days)
Falkovich et al. (2001)	C Q F G	Total	Tel-Aviv, Israel	03/16/1998
Ferguson et al. (1970)	M K S O	< 2 µm	Northeasten Pacific	April 1969
Fiol et al. (2005) [d]	M K C Q F O	Total	Palma de Mallorca, Spain	05/06/1988– 04/27/1999
Formenti et al. (2008)	M K C Q F[e]	< 40 µm	Banizoumbou, Niger	01/13/2006– 02/13/2006
Game (1964)	C Q F I O	Total	East Atlantic	02/06/1962
Ganor (1991)	M K O	< 10 µm	Tel Aviv and Jerusalem, Israel	1968–1987
Ganor et al. (2000)	1:M K S O 2:C Q F	1: < 2 µm 2: >= 2 µm	16 locations around Lake Kinneret, Israel	01/1993–05/1997
Gaudichet et al. (1989)	M K S C Q F O	Total	Amsterdam Island, TAAF	05/15/1994– 05/26/1984, 07/07/1984– 07/30/1984, 09/05/1984– 09/29/1984

ACPD
15, 3577–3627, 2015

Predicting the mineral composition of dust aerosols – Part 2

J. P. Perlwitz et al.

Table 1. Continued.

Reference	Minerals	Size Range	Location	Time Range
Gaudichet et al. (1992)	M K S O	< 2 µm	1: Vostok, 2: South Pole	1: 1927 2: 1955
Glaccum and Prospero (1980)	M K C Q F O	Total	Sal Island, Cape Verde; Barbados; Miami, Florida	07/1974–08/1974
Goldberg and Griffin (1970)	M K S O	< 2 µm	1: Bay of Bengal 2: Waltair, India	1: 05/1968 2: 01/1969
Jeong (2008)	M K S C Q F O	< 10 µm	Seoul, Korea	Spring 2003, 2004, 2005
Jeong and Achterberg (2014)	M + S K C Q F G O	< 60 µm	1: Deokjeok Island, Korea 2: Andong, Korea 3: São Vicente, Cape Verde	1: 03/31/2012[f] 2: 03/16/2009–03/17/2009[f], 03/20/2010[f], 03/18/2014[f] 3: 12/28/2007–12/31/2007, 01/18/2008–01/23/2008
Jeong et al. (2014)	M + S K C Q F I G O	1: 5 size bins up to 60 µm 2: < 60 µm	1: Deokjeok Island, Korea 2: Andong, Korea	1: 03/31/2012–04/01/2012[f] 2: 03/20/2010[f], 05/01/2011[f]
Johnson (1976)	1: M S O 2: M + K + S[g] Q F	1: < 2 µm 2: Total	3 in Atlantic; Barbados	12/1898; 10/1965; 03/1971
Kandler et al. (2007)	M C Q F I G O	8 size bins 0.05 to 20 µm[h]	Izaña, Tenerife, Canary Islands, Spain	07/13/2005–07/23/2005, 08/06/2005–08/08/2005
Kandler et al. (2009)	M K C Q F I G O	10 size bins 0.1 to 250 µm[i]	Tinfou, Morocco	05/13/2006–06/07/2006

Discussion Paper | Discussion Paper | Discussion Paper | Discussion Paper |

ACPD
15, 3577–3627, 2015

Predicting the mineral composition of dust aerosols – Part 2

J. P. Perlwitz et al.

Table 1. Continued.

Reference	Minerals	Size Range	Location	Time Range
Kandler et al. (2011)	M[j] K S C Q F G O	Total	Praia, Cap Verde	01/14/2008–02/09/2008 (daily)
Khalaf et al. (1985)	M + S K C Q F G O	< 4 µm	8 location in Kuwait	04/1979–03/1980
Leinen et al. (1994)	M K S Q F O	1: < 2 µm; 2: 2–20 µm	Northwest and East Pacific	09/1977–10/1979
Lu et al. (2006)	M K S Q F O	< 10 µm	Beijing, China	04/2002–03/2003
Menéndez et al. (2007)	M K[k] C Q F O	Total	Gran Canaria, Canary Islands, Spain	10/31/2002–10/23/2003
Møberg et al. (1991)	M K S Q F I O[l]	< 2 µm	Zaria, Nigeria	11/1984–03/1985
O'Hara et al. (2006)	M K C Q F G O	Total	1: Northern Libya 2: Southern Libya	06/2000–05/2001
Parkin et al. (1970)	M S Q O	Total	North Atlantic	01/1969 and 08/1969
Parkin et al. (1972)	M S Q O	Total	Central Atlantic	02/1971–03/1971
Prospero and Bonatti (1969)	M K S Q F O	< 20 µm	East Pacific	Spring 1967
Prospero et al. (1981)	M K Q F C I G O	Total	1: Cayenne 2: Dakar, Barbados, Cayenne	1: 12/1977–04/1980 2: 03/21/1978–03/27/1978
Queralt-Mitjans et al. (1993)	M K C Q F G O	Total	7 locations at Filabres Range, Spain	11/1989–12/1989, 03/1990–05/1990
Rashki et al. (2013)	M C Q F G O	< 75 µm	2 locations in Sistan Region, Iran	08/2009–08/2010
Shao et al. (2008)	1: M K S[m] O 2: M + K + S C Q F G O	1: < 2 µm 2: Total	Beijing, China	1 + 2: 04/17/2006, Spring 2006 2: Spring 2004, 2005
Shen et al. (2006)	M K C Q F O	Total	Dunhuang, China	Spring 2001 and 2002
Shen et al. (2009)	M C Q F O	Total	5 locations in desert regions of China	Spring 2001 and 2002

ACPD
15, 3577–3627, 2015

Predicting the mineral composition of dust aerosols – Part 2

J. P. Perlwitz et al.

Table 1. Continued.

Reference	Minerals	Size Range	Location	Time Range
Shi et al. (2005)	1: M K S O 2: M + K + S C Q F I G 3: M + K + S C Q F O	1: < 2 µm 2: < 10 µm 3: Total	Beijing, China	04/06/2000 and 03/20/2002 (1 and 2 only)
Skonieczny et al. (2013)	M K S O[n]	< 30 µm	Mbour, Senegal	02/23/2006–03/27/2009 (weekly)
Tomadin et al. (1984)	M K S O	< 2 µm	1: Central Mediterrenean 2: Central Mediterrenean 3: Scilla, Messina, Bologna	1: 03/1981 2: 10/1981–11/1981 3: 03/1981
Windom (1969)	M K S Q F O	Total	5 permanent snow fields on planet	before 1969
Zdanowicz et al. (2006)	M K S O	Total	St. Elias Mountains, Canada	04/16/2001
Zhou and Tazaki (1996)	I + K + S C Q G O	Total	Matsue, Japan	10/1992–09/1993 (weekly)

[a] only Red Rain events;
[b] may contain chlorite;
[c] may contain rutile or pyrolusite;
[d] only Red Rain events;
[e] all minerals: percentage of refractive surface (XRD);
[f] dust event;
[g] includes chlorite;
[h] used here: 1–2.5, 2.5–5, 5–10, and 10–20 µm ranges;
[i] interpolated to ModelE size bins;
[j] as part of mixed layer illite-smectite;
[k] kaolinite-chlorite;
[l] all minerals: from maximum and minimum value;
[m] as part of mixed-layer illite-smectite;
[n] mineralogy of aluminosilicates only.

ACPD
15, 3577–3627, 2015

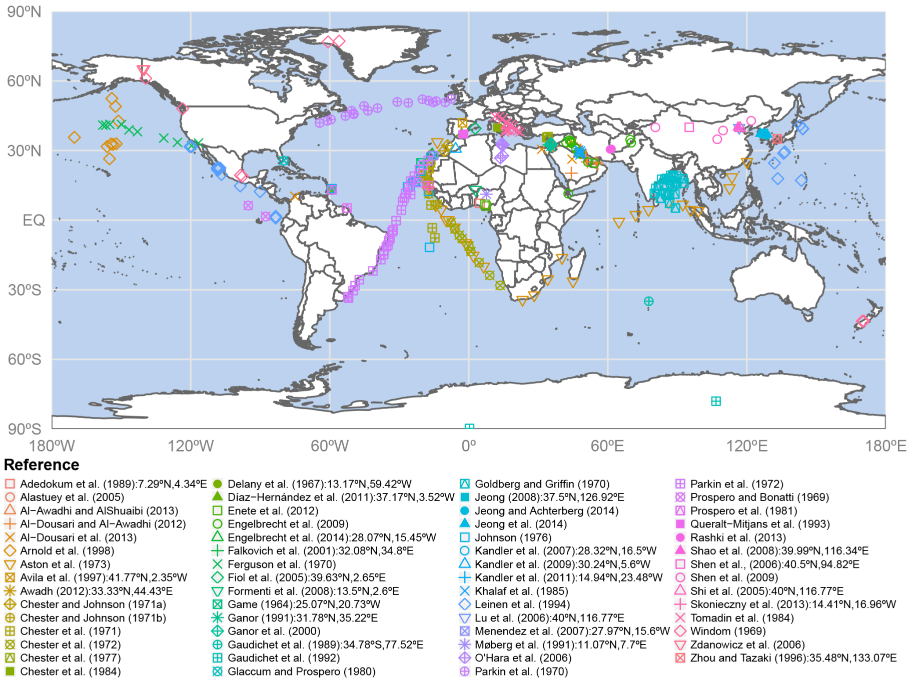

Figure 1. Locations of measured mineral fractions compiled from the literature used for the evaluation of the simulations. References with geographical coordinates in the legend provide measurements only for this single location; otherwise, references provide measurements for multiple locations. See Table 1 and Table S1 in the Supplement for more information.

ACPD
15, 3577–3627, 2015

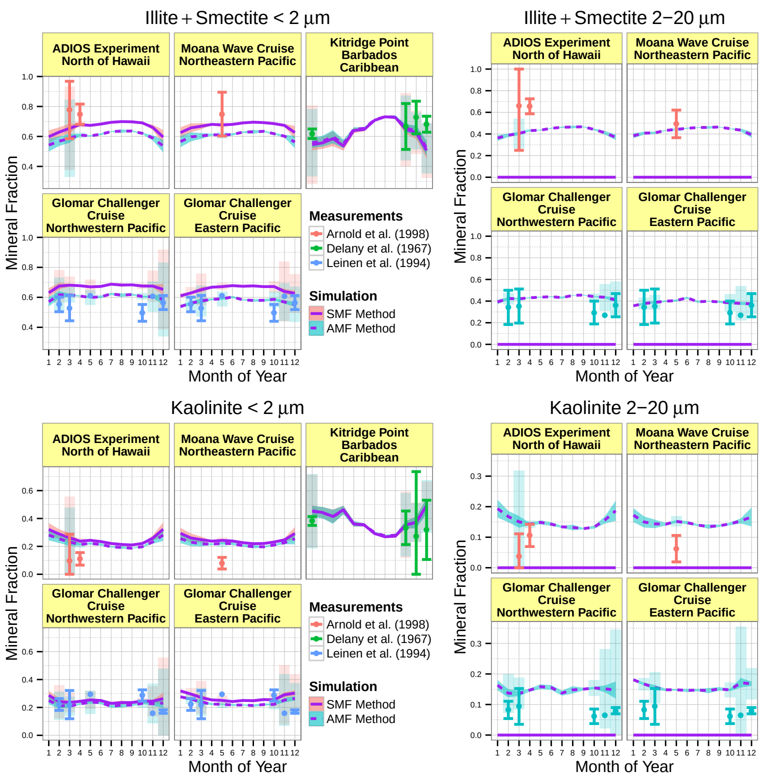

Figure 2. Annual cycle of illite plus smectite and kaolinite fractions for diameters less than 2 µm and from 2 to 20 µm as measured and simulated by the SMF and AMF methods. The vertical error bars, shaded ribbons, and shaded bars represent the 95 % confidence intervals of the measurements, the simulations (based on monthly SDs), and the simulations sampled at the frequency of the measurements, respectively.

ACPD
15, 3577–3627, 2015

Predicting the mineral composition of dust aerosols – Part 2

J. P. Perlwitz et al.

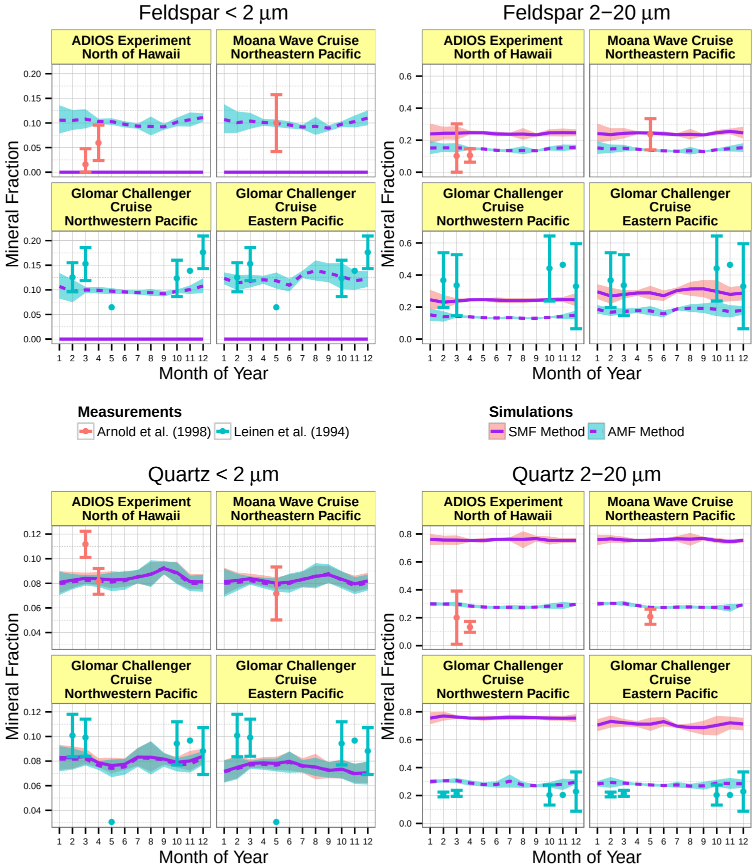

Figure 3. Same as Fig. 2 but for feldspar and quartz.

ACPD
15, 3577–3627, 2015

Predicting the mineral composition of dust aerosols – Part 2

J. P. Perlwitz et al.

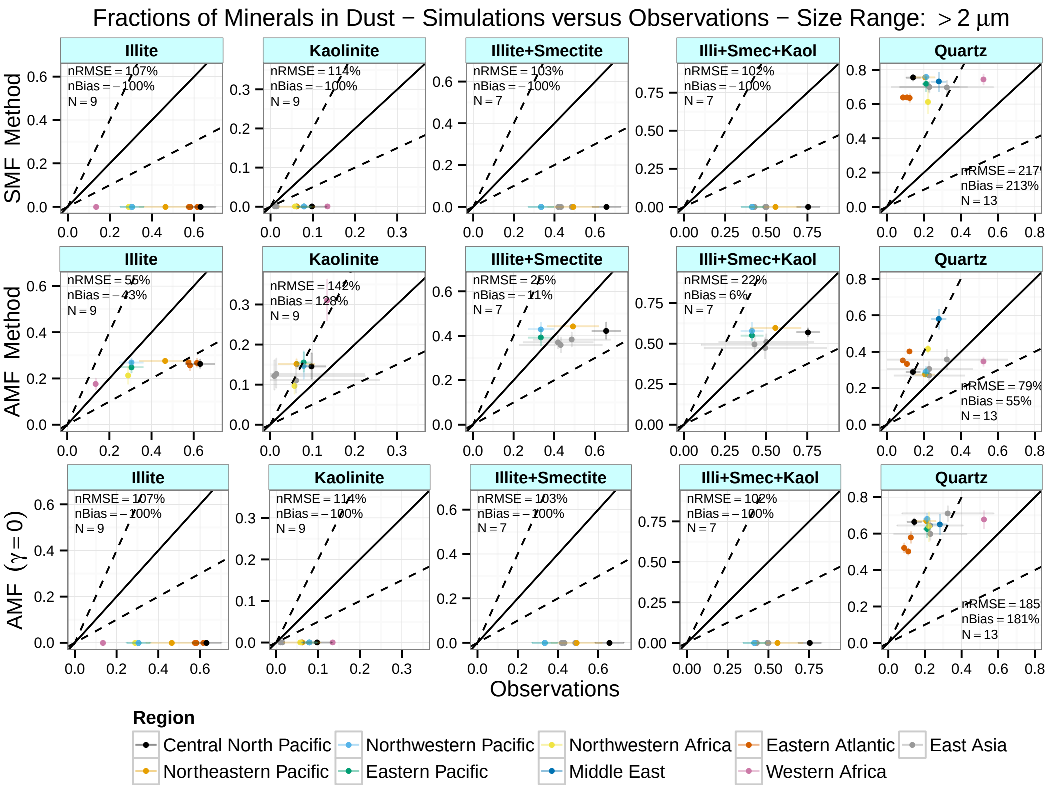

Figure 4. Scatter plot of mineral fractions of illite, kaolinite, the sum of illite and smectite, all phyllosilicates and quartz for silt particles (whose diameters are greater than 2 µm) simulated by the SMF, AMF and AMF ($\gamma = 0$) experiments vs. measurements. The dashed lines mark ratios of 2 : 1 and 1 : 2 between simulated and observed mineral fractions. The horizontal and vertical error bars show the 95 % confidence intervals.

ACPD
15, 3577–3627, 2015

Predicting the mineral composition of dust aerosols – Part 2

J. P. Perlwitz et al.

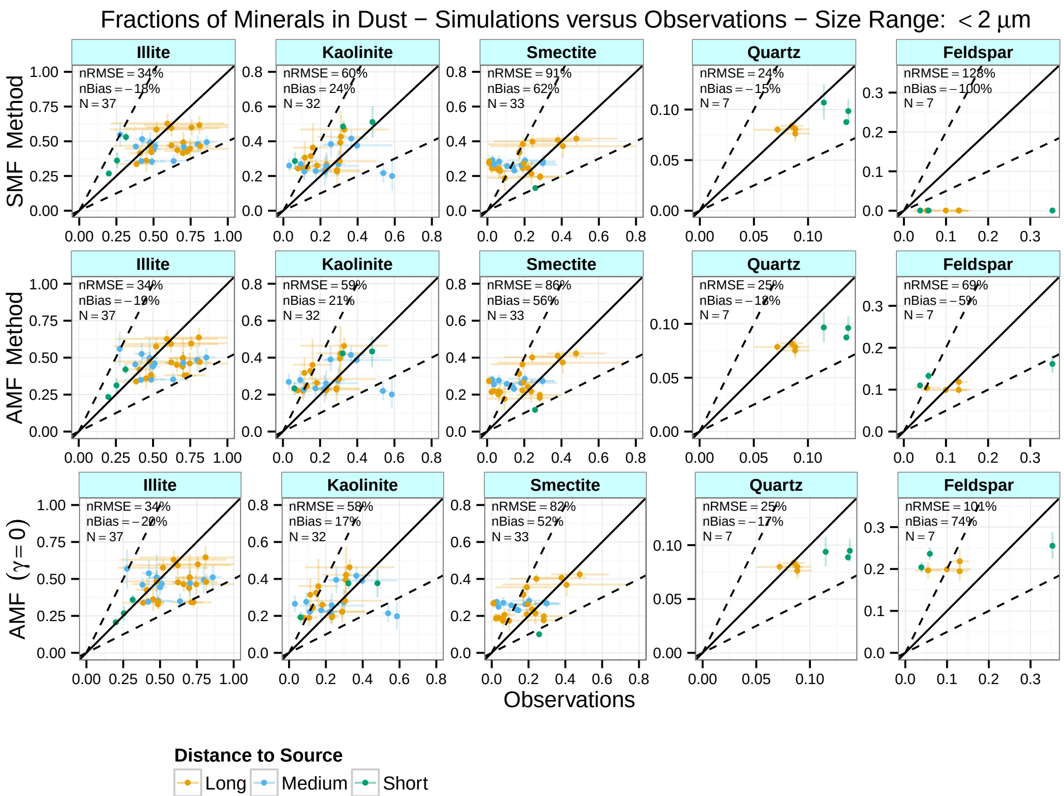

Figure 5. Same as Fig. 4 but for illite, kaolinite, smectite, quartz, and feldspar at clay diameters (less than 2 µm).

ACPD
15, 3577–3627, 2015

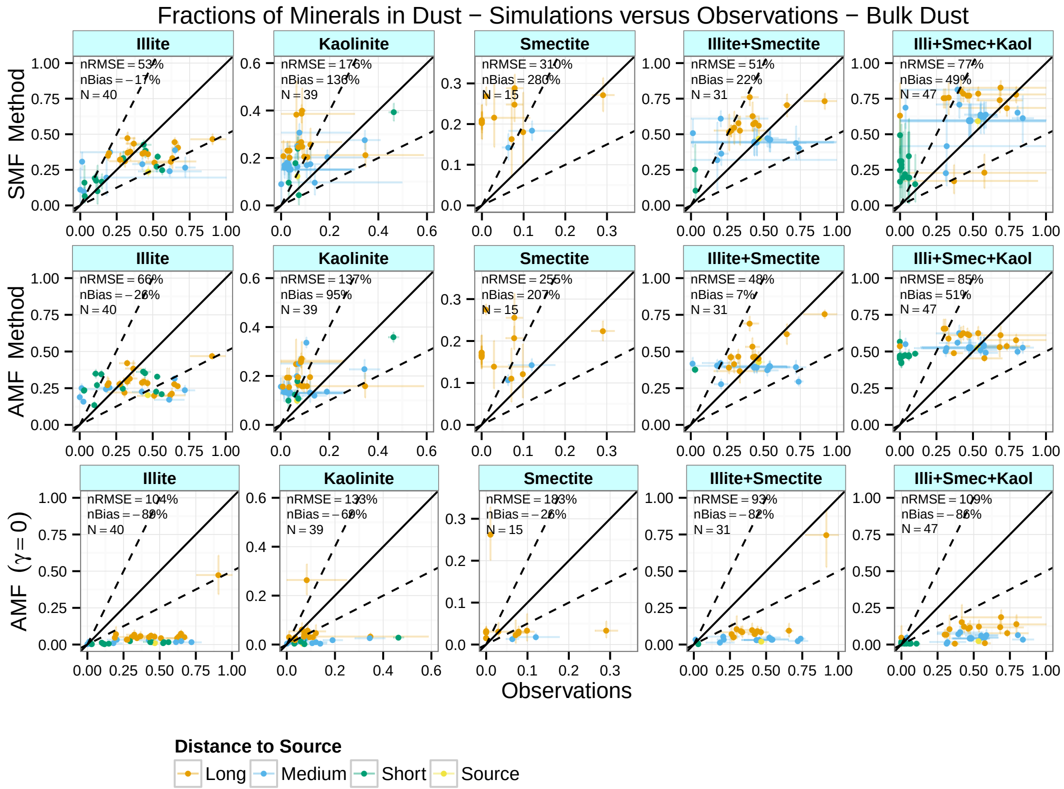

Figure 6. Same as Fig. 4 but for bulk (clay plus silt) mineral fractions of illite, kaolinite, smectite, the sum of illite and smectite, and all phyllosilicates.

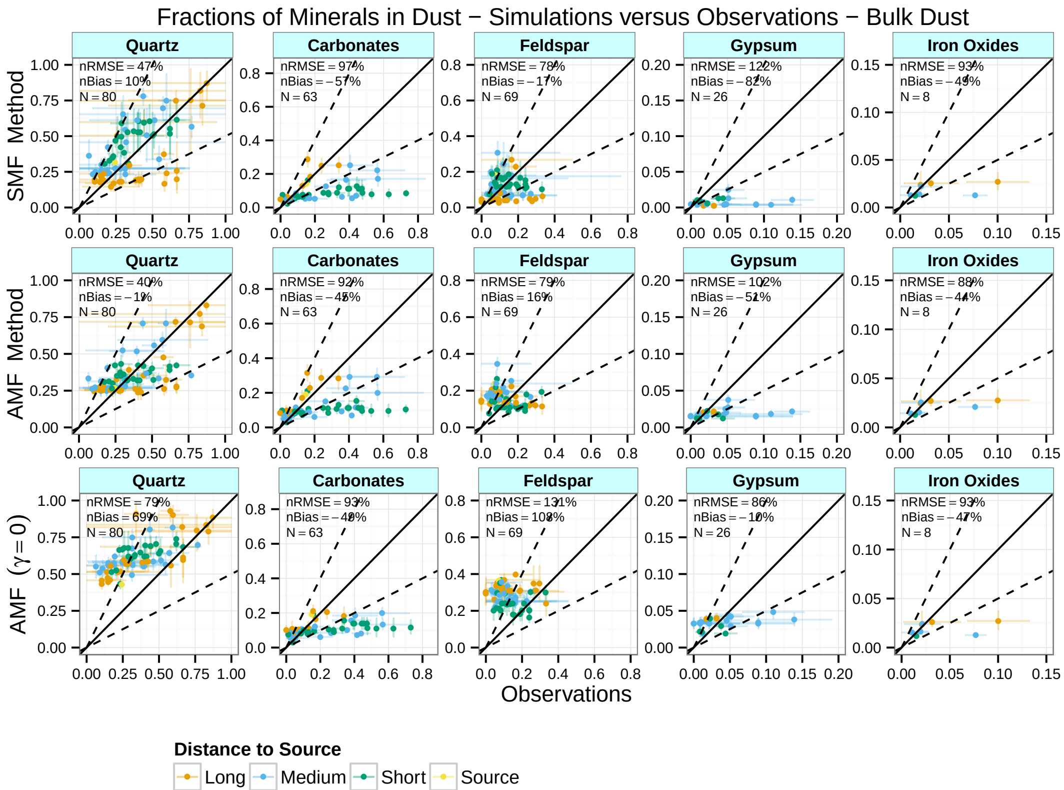

Figure 7. Same as Fig. 4, but for bulk mineral fractions of quartz, carbonates, feldspar, gypsum, and iron oxides.

ACPD
15, 3577–3627, 2015

Predicting the mineral composition of dust aerosols – Part 2

J. P. Perlwitz et al.

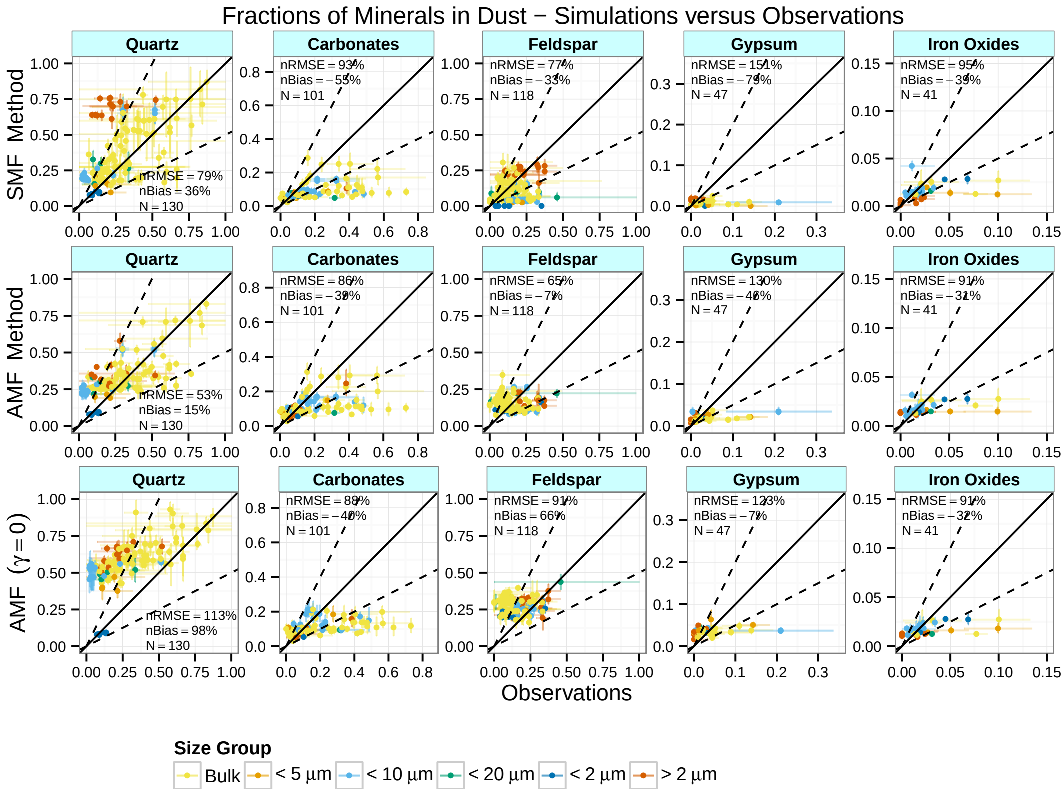

Figure 8. Same as Fig. 4, but including particle mass (PM) measurements at other size ranges.

ACPD
15, 3577–3627, 2015

Title Page
Abstract | Introduction
Conclusions | References
Tables | Figures
◀| |▶
◀ ▶
Back | Close
Full Screen / Esc
Printer-friendly Version
Interactive Discussion

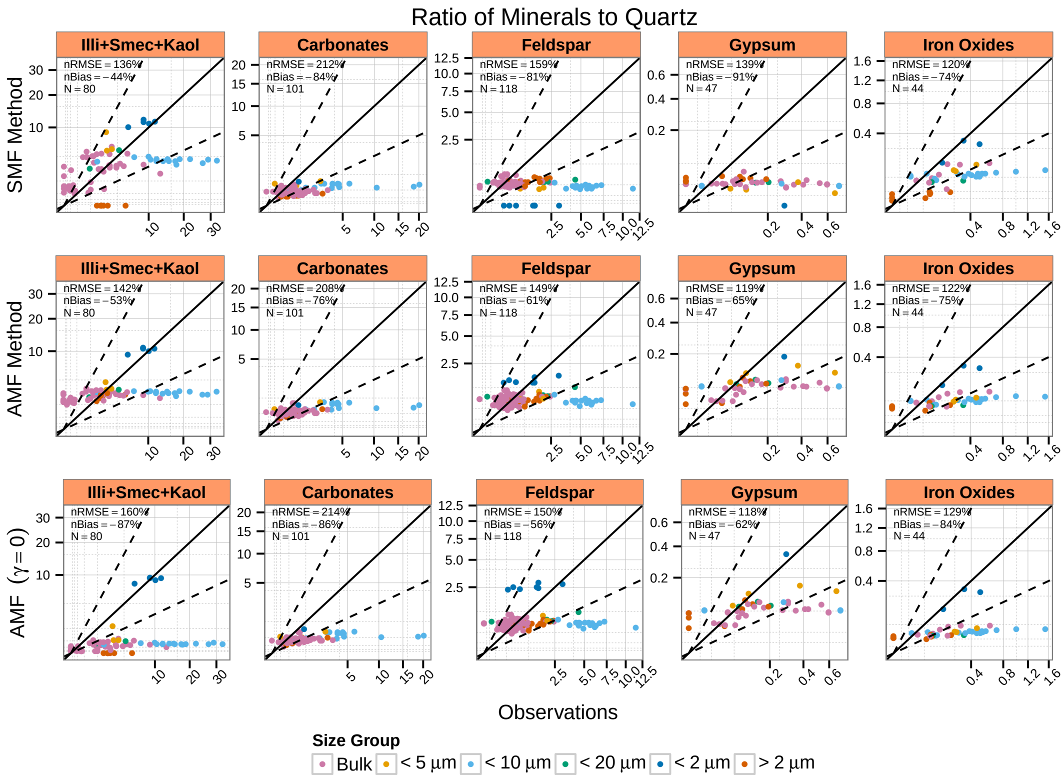

Figure 9. Measured vs. simulated mineral ratios with respect to quartz for the SMF, AMF and AMF ($\gamma = 0$) methods. The dashed lines mark a ratio of 2 : 1 and 1 : 2 between simulated and observed mineral ratios.

ACPD
15, 3577–3627, 2015

Predicting the mineral composition of dust aerosols – Part 2

J. P. Perlwitz et al.